fibers MDPI

Article

Constitutive Model for Plain and Steel-Fibre-Reinforced Lightweight Aggregate Concrete Under Direct Tension and Pull-Out

Hasanain K. Al-Naimi [1] and Ali A. Abbas [2]

University of East London
* Correspondence:
[1] Doctoral Graduate, MEng, MSc, PhD
[2] Associate Professor of Structural Engineering, BSc(Eng), DIC, PhD

Abstract: In the present study, a programme of experimental investigations was carried out to examine the direct uniaxial tensile (and pull-out) behaviour of plain and fibre-reinforced lightweight aggregate concrete. The lightweight aggregates were recycled from fly ash waste, also known as Pulverised Fuel Ash (PFA), which is a by-product of coal-fired electricity power stations. Steel fibres were used with different aspect ratios and hooked ends with single, double and triple bends corresponding to DRAMIX steel fibres 3D, 4D and 5D types, respectively. Key parameters such as the concrete compressive strength f_{lck}, fibre volume fraction V_f, number of bends n_b, embedded length L_E and inclination angle θ_f where considered. The fibres were added at volume fractions V_f of 1% and 2% to cover the practical range and a direct tensile test was carried out using a purpose-built pull-out test developed as part of the present study. Thus, the tensile mechanical properties were established and a generic constitutive tensile stress-crack width σ–ω model for both plain and fibrous lightweight concrete was derived and validated against experimental data from the present studies and also previous research found in the literature (including RILEM uniaxial tests) involving different types of lightweight aggregates, concrete strengths and steel fibres. It was concluded that the higher the number of bends n_b, volume fraction V_f, and concrete strength f_{lck}, the stronger the fibre-matrix interfacial bond and thus the more pronounced the enhancement provided by the fibres to the uniaxial tensile residual strength and ductility in the form of work and fracture energy. A fibre optimisation study was also carried out and design recommendations made.

Keywords: lightweight concrete; hooked-end steel fibres; constitutive tensile s-w model; uniaxial tensile behaviour; pull-out behaviour; fracture energy; ultimate bond strength; fibre optimisation

1. Background Review

1.1 *Lightweight Aggregate Concrete*

Recently, there has been a rapid growth in concrete technology that is particularly directed towards sustainability and upgrading strength-to-weight ratio 1. Achieving the latter results in reduction in building mass which leads to savings in materials, construction time and – crucially – reduction in costs and adverse effects of carbon emissions (including in the transportation of less materials). Therefore, the use of structural lightweight aggregate concrete (LWAC) as a replacement to the conventional heavier normal weight concrete (NWC) counterpart helps achieve such goals. In addition, the lightweight aggregate used in this work is made from recycled waste and thus offers further reduction in CO_2 emissions as well as being an alternative to depleting quarried natural resources 2. The recycled aggregates are made from fly ash waste (commonly known as LYTAG), which is a by-product of coal-fired electricity power stations 3. Fly ash, also termed Pulverised Fuel Ash (PFA) is the ash resulting from the burning of pulverised coal in these power stations. Several studies support the environmental benefits provided by this PFA-based material and its effectiveness in reducing carbon emissions 4. Additionally, it should be noted that LWAC brings other advantages such as increased thermal insulation, noise absorption and fire resistance 5,6. Thus, the use of lightweight concrete can allow for taller and longer span structures and is also beneficial in situations when reduction of inertial loads is needed such as in seismic zones 7,8,9,10. Nonetheless, despite these benefits, some disadvantages have been highlighted with the use of LWAC. One of the key shortcomings is the increased brittleness of lightweight concrete in comparison to the normal weight counterpart, which is likely due to the porous concrete matrix and its poor aggregate interlock mechanism. This leads to a complete absence of strain softening mechanism post cracking 2. Therefore, for plain LWAC, instantaneous failure is observed both in compression and tension at the *material* level once peak stress is reached. Similarly, a drastic reduction in shear capacity, excessive deflection and cracking due to the lower modulus of elasticity is expected at the *structural* level 11,12,13,14. Despite the fact that modern structural LWAC has been around for over several decades, its mechanical properties have not been comprehensively researched, and the material and structural equations defining its behaviour have been traditionally adapted from dated studies on NWC 15,16,17,18,12,14.

1.2 Steel Fibres

To address the increased brittleness of LWAC, steel fibre reinforcement has emerged as a potential solution whose effectiveness has been proven in increasing ductility of other fibrous composites in the past 19,20,21,22,23. This is because one of the key benefits to steel fibres is enhancement to ductility. Their key advantage over conventional bar reinforcement is the reduction in construction time, as they can conveniently be added to the concrete ready mix delivered, hence leading to economic and environmental benefits. Steel fibre reinforced concrete (SFRC) is also particularly useful for smaller cross-sectional elements and for sprayed concrete, e.g. shotcrete, which is commonly used in tunnel lining. Another potential application is to relax the shear reinforcement spacing at beam ends [24] and in critical elements in seismic-resistant design such as beam-column joints [25], which can get congested with conventional bar reinforcement leading to practical construction difficulties. Hooked-end steel fibres are the most commonly used type and are usually made by cutting steel wire into short lengths and then cold-drawing them to create a hook shape at one end. This type of steel fiber is mainly used in structural applications due to its improved bond properties with concrete (compared to straight fibres without ed hooks). The bond can be enhanced further by increasing the number of end hooks. The present study examines the performance of single and multiple end hook arrangements. Straight steel fibres on the other hand have a smooth surface that reduces friction (and bond with concrete as a consequence). They are usually used in thin concrete structures such as precast concrete panels and overlays, and in applications with less demanding structural performance.

Although somewhat limited, research studies on fibrous lightweight concrete have been reported for several years 26. However, at present, there are hardly any international standards specific to steel fibre reinforced lightweight concrete (SFRLC) with current guidelines being usually adapted from fibrous normal weight concrete (SFRC). The practical application of steel fibre reinforcement in lightweight concrete is still in its infancy, is largely carried out at the *structural* level only in the form of case studies that largely involved lightweight aggregates (such as pumice stone and oil palm aggregates) different to the ones investigated in the present research work 22,23,27,28,29. The recycled PFA-based aggregates used herein are well established for structural use by the construction industry, so they represent a good benchmark to test the addition of fibres and mean that the ensuing findings and recommendations will be useful to current practice. It should also be borne in mind that coal-fired power generation remains the largest contributor of energy in the world 32, even with decommissioning of coal plants there is still large historical waste. Therefore, the present comprehensive study on fibrous recycled PFA-based lightweight aggregate concrete is particularly beneficial in providing sustainable design solutions for the rapidly developing fibrous concrete technology. The present study is part of a large experimental programme which examined the structural behaviour of steel-fibre-reinforced recycled PFA-based lightweight concrete at both the *material* and *structural* levels [30]. The compression structural responses of SFRLC were examined in an earlier publication [31]. The present article is focused on the series of tests that were carried out to investigate the uniaxial tensile and pull-out behaviour of lightweight concrete reinforced with different hooked-end steel fibres at fibre volume fraction V_f of 1% and 2%.

1.3 Tensile Behaviour and Limitations of Existing Research

Under tensile loading, as the principal tensile stress applied exceeds the ultimate tensile resistance of plain concrete, microcracks start to form and morph into a single larger macrocrack, which eventually leads to concrete failing in tension, thus releasing the stored energy of the system 33. When fibres are added, a crack-arresting action takes place once cracks have formed, then fibres create a bridge between the ends of the crack to resist its extension. However, as the principal tensile stress grows and due to sliding friction, the fibres may end up being pulled-out or ruptured depending on the number of fibres crossing the crack (which providing a good mixing process, usually correlates with the fibre volume fraction V_f) and the fibre-matrix interfacial bond strength. The latter is largely governed by the geometry of fibre, its tensile strength, mechanical anchorage, embedment length, inclination angle and concrete strength. These factors govern the post-crack behaviour of fibrous concrete. Researchers such as Löfgren 34 and Lee *et al.* 35 detailed this behaviour for fibrous normal weight concrete, which benefits from the combined effect of fibre reinforcement and residual effect of aggregate interlock mechanism once crack develops. Given that the aggregate interlock mechanism is expected to be negligible for lightweight concrete, this effect might be different for fibrous lightweight concrete in the post-cracking phase.

Indirect tensile tests to investigate the flexural tensile behaviour of fibrous concrete can be found in the literature 7,19,27,29,36,37,38,39. It is established that the addition of steel fibres upgrades the flexural behaviour of lightweight concrete. However, the uniaxial tensile behaviour of fibrous lightweight concrete has not been thoroughly investigated to establish analytical models. This important aspect has been addressed in the present research work because, unlike flexural testing, the direct uniaxial tensile testing offers the ideal results required to understand the tensile pre- and post-cracking behaviour of concrete and the interaction of LWAC with fibres. Currently, limited comprehensive studies were found in the literature that is focused on the investigation of the uniaxial tensile stress-strain (σ-ε) or stress-crack width (σ-ω) behaviour and pull-out behaviour of SFRLC. Amongst all available research examined, it seems that only Grabois *et al.* 23 and Mo *et al.* 40 carried out direct uniaxial tensile tests on lightweight concrete using dog-bone test [41] and RILEM TC 162-TDF uniaxial test 42, respectively. They reported an increase of uniaxial tensile residual strength with hooked-end steel fibre reinforcement with $V_f \leq 0.5\%$ and $V_f < 1\%$ compared to plain LWAC, respectively. Grabois *et al.* 23 showed a stress-strain relationship while Mo *et al.* 40 only estimated the tensile strength. Moreover, there seems to be a lack of thorough investigation on pull-out tensile behaviour of fibrous PFA-based lightweight aggregate concrete, especially with modern multi-bend fibres like the ones used in the prrsent study.

Therefore, the present research work serves to offer more clarity and understanding on the uniaxial tensile and pull-out behaviour of steel-fibre-reinforced lightweight concrete and presents valuable additional experimental data to enrich the current available literature. This culminated in derving tensile properties including tensile σ-ω constituitive models for SFRLC, fracture energy G_f and bond strength. It also led to the development of a fibre optimisation study based on different hooked-end steel fibre types, geometries and contents and plain lightweight concrete compressive strengths.

3. Experimental Study

The mixing process, materials, grading, vibration, curing and specimen preparation were all detailed in a preceding paper, which was focused on the compression behaviour of SFRLC [31] as part of a comprehensive experimental research programme [30]. For the sake of completeness and to avoid repetition, only new data are presented herein.

3.1. Material Properties

The material chemical and geometrical properties of cement, natural sand and PFA-based coarse aggregates used in the experiments were detailed elsewhere [30,31].

Recycled sintered pulverised fly ash aggregates were used as the coarse aggregate of the lightweight concrete in the present experimental study. The fly ash is a by-product of coal-fired electricity power stations 3. The aggregates (4-14 mm) are brown, roughly spherical with a honeycomb structure of interconnected voids. They have a specific gravity of about 1.8 and water absorption of up to 15%. Natural sharp sand with a maximum aggregate size of 4.75 mm was used as the fine aggregate of the concrete. In the present study, Dramix hooked-end (single-bend) 3D fibres with different aspect ratios were incorporated as reinforcement for the pull-out specimens. The fibres tested in this work are shown in **Error! Reference source not found.**, while their geometrical properties which were adapted from Abdallah *et al.* 43,44 are shown in **Error! Reference source not found.**. A schematic representation of the parameters shown in **Error! Reference source not found.** is depicted in **Error! Reference source not found.**. It should be noted that hooked-end 3D fibres were regarded as the control fibres during the experimental programme. The rest of the fibres were used in order to evaluate the effects of different fibre geometries, bends, lengths and diameters on the behaviour of lightweight concrete.

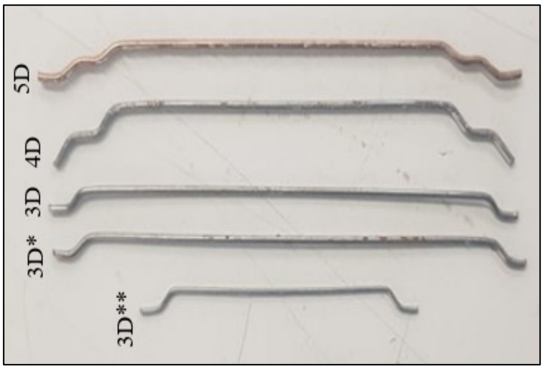

Figure 1. Fibres used in this work.

Table 1. Properties of hooked-end fibres used 45. Geometrical properties of hooks are adapted from 43 and 44.

Fibre Type	σ_u (MPa)	e_u (%)	*E* (GPa)	σ_y (MPa)	L_f (mm)	d_f (mm)	L1 (mm)	L2 (mm)	L3 (mm)	L4 (mm)	θ_1 (°)	θ_2 (°)	β (°)
3D	1160	0.8	210	775-985	60	0.9	2.12	2.95	-	-	45.7	-	67.5
3D*	1225	0.8	210	775-985	60	0.75	-	-	-	-	-	-	-
3D**	1345	0.8	210	775-985	35	0.55	2.55	2.22	-	-	38.3	-	70.9
4D	1500	0.8	210	1020 -1166	60	0.9	2.98	2.62	3.05	-	30.1	30.8	75
5D	2300	6	210	1177-1455	60	0.9	2.57	2.38	2.57	2.56	27.9	28.2	76

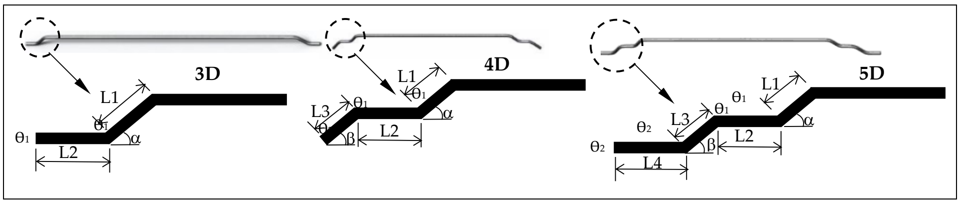

Figure 2. Schematic representation of parameters shown in **Error! Reference source not found.** (adapted from 43).

3.2. Properties of Mixes

In addition to the 4 mixes cast in the preceding study on compressive behaviour [30,31], mixes 1-3D* and 1-3D** were added with fibres 3D* and 3D**, respectively (as summarised in **Error! Reference source not found.**).

Table 2. Mix design.

Mix	V_f (%)	Fibre	$f_{lck}/f_{lck,cube}$	Cement (kg/m³)	Sand (kg/m³)	PFA-based aggregates (kg/m³)	Effective water (kg/m³)
1-3D		**3D**	**LC30/33**	370	592	635.6	175

1-3D*	1-2 (80-160kg/m^3)	**3D***						
1-3D**		**3D****						
1-4D		**4D**						
2		**3D**	**LC35/38**	420	546			
3		**5D**	**LC40/44**	480	485			

3.3. Test Method for Pull-Out Test

In this section, the details of the design and method of uniaxial tensile pull-out tests on notched prisms are provided. Uniaxial compression cube and cylinder tests with their setups and instrumentations were detailed in an accompanying paper [30,31]. For the pull-out tests, each mix included two repeated notched prisms specimens per volume fraction V_f dosage. Building on the previous experimental study by Robins *et al.* 46, a direct uniaxial tensile pull-out test was designed in the present study, which can be used for both plain and fibrous concrete. The aim was to investigate the effect of the embedded fibres on the uniaxial tensile stress-crack width response of lightweight concrete. The main difference between the test setup proposed herein and the one by Robins *et al.* 46 is that for the latter the steel fibre is embedded in concrete on one end and in a high strength mortar on the other end, to grip the fibres and practically prevent their movement on that side, while the fibre in the proposed test setup is embedded in the lightweight concrete matrix on both ends. Hence, Robins *et al.* test 46 is practically similar to the conventional single fibre pull-out test shown in other previous studies 47,48,49.

The designed uniaxial tensile pull-out test adopted in this work (depicted in **Error! Reference source not found.**) carries several advantages. First, it mimics to a large extent a truer representation of the behaviour of steel fibres bridging a crack in a real structural element as compared to the classic pull-out tests explained earlier, since fibres are completely embedded in lightweight concrete, while the crack is not predefined but induced by a reduced section (notch) spanning 10 mm in the middle of the specimen. The reason for designing this notch is to allow continuity of lightweight concrete constituents of the specimen (sand, PFA-based aggregates and cement) through the notch at which breakage is thus ensured. Also, the notch allows the introduction of embedment length L_E as a variable and enables the specimen to be monitored in the middle section in terms of load-slip behaviour. Since the crack is not predefined, it was possible to derive LWAC and SFRLC peak tensile cracking load when the behaviour is elastic. Secondly, by taking into consideration V_f in the effective area of the cylinder around the embedded fibre, this test can be regarded as both a fibre pull-out and a uniaxial tensile test. Similarly to the previous experimental study by Robins *et al.* 46, the effective area of the notched cylinder through which the fibre is embedded was determined using numerical and statistical models which depend mainly on fibre geometry and fibre volume fraction 50,5152. Thereby, the diameter of the notch was calculated to be 12 mm and is corresponding to V_f = 1% for DRAMIX hooked-end fibres of d_f = 0.9 mm (3D, 4D and 5D). It should be noted that to test the concrete for V_f = 2%, simply another fibre was added. The fibre spacing was equal in the notch.

Figure 3. Proposed notched prism being tested in the direct uniaxial tensile pull-out machine.

Based on the concrete fibre-matrix interfacial properties which are directly affected by the densification of the matrix and water/cement (w/c) ratio of concrete (which influence the compressive strength), fibre content V_f, aspect ratio a_f, mechanical anchorage (number of bends or hooks), embedment length L_E, orientation angle, dispersion and tensile strength 464953,54, the stress-crack width relationship was derived. The aforementioned factors govern the bond-slip behaviour between concrete and fibres, which in turn influences the tensile behaviour both at the *material* and *structural* levels of SFRLC. Hence, the evaluation of the results of this test explicitly enable the prediction of the behaviour of SFRLC members such as beams and slabs. It should be noted that 2 moulds with different dimensions were designed to test 2 different types of pull-out notched prism specimens for each mix (shown in **Error! Reference source not found.**). The pull-out notched prism specimens were produced using both moulds A and B.

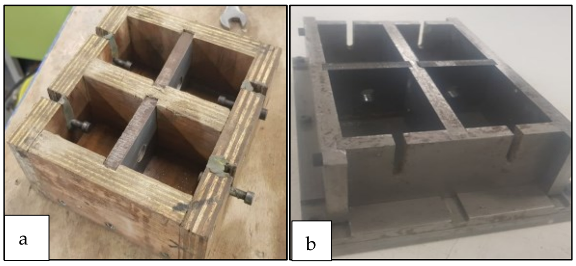

Figure 4. a- Mould (A) and b- Mould (B).

Each mould contained 2 identical chambers. The differences in dimensions between mould A and B are shown in **Error! Reference source not found.**. The reason behind testing 2 different types of notched prisms in pull-out was to ensure developing an accurate and realistic stress-crack width relationship of fibrous lightweight concrete independent of the size effects of the specimen used and thus can be applied to any structural member. Preliminary trials showed that both moulds yielded similar results for identical specimens in terms of pull-out load-slip behaviour and failure patterns. Therefore, the stress-crack width relationship derived based on these tests can be applied directly to FE models unlike the more common stress-strain relationship which usually requires calibration or the study of the structural characteristic length l_{cs}, which is used to derive strain ε with $\varepsilon = \omega/l_{cs}$. To prepare the pull-out specimen before casting, the fibre was positioned at the notch for the chosen L_E and the required inclination angle to the load, using fixed fine suspended cables mechanically attached to the fibre. These were removed once concrete was cast to avoid any potential interference with the results.

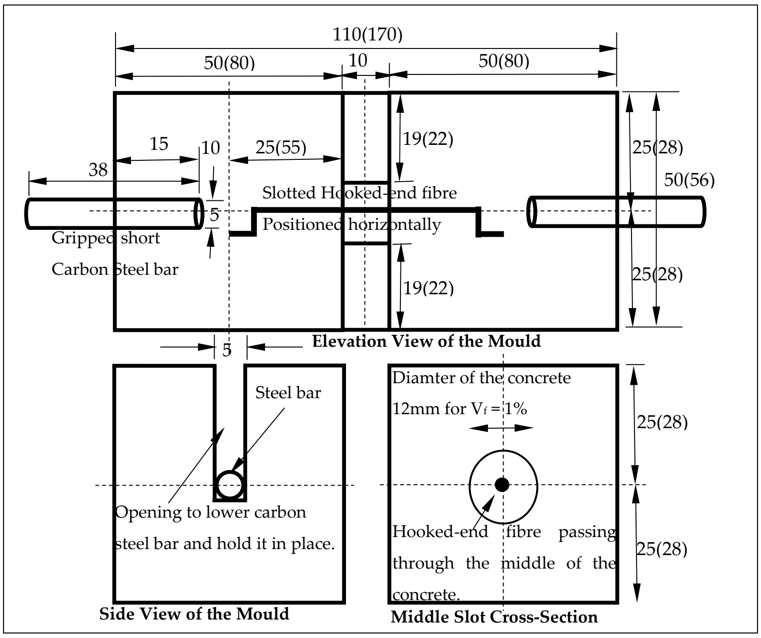

Figure 5. The dimensions of 1 chamber in pull-out mould A and B. Values between brackets are for mould B dimensions only. All dimensions are in (mm).

During the pull-out test photographed in **Error! Reference source not found.**, as the 2 short rigid carbon steel bars (embedded at the ends of the specimen) were being pulled in opposite directions using machine grips, the cylindrical concrete volume through which the fibre was embedded became subjected to pure unidirectional tension. The embedded carbon steel bars had enlarged ends and were further prevented from potential slip with steel washers attached to their heads. Although possible slip of small steel bars might occur before concrete cracking, both concrete blocks embedding the two hooked ends of the fibre were assumed to be rigid following concrete cracking. Since the bond of the carbon steel bar with the lightweight concrete matrix is higher than that of hooked-end steel fibres, the pull-out response of the fibrous lightweight concrete specimen was designed to only occur along the fibre and the surrounding concrete. These assumptions were found to be correct, as shown in the results section. The tensile machine was calibrated and fitted with a sensitive displacement transducer capable of accurately measuring the slip once the crack was initiated. The pull-out specimen was carefully placed in the tensile testing machine with a maximum load cell capacity of 20 kN, where the two carbon steel bars from each end were securely gripped in a way to disallow any superfluous slip. While one end was fixed, the other end was gradually pulled in tension at a displacement-controlled loading rate of 1 mm/min with 2 readings recorded every 1 sec.

Cao and Yu 55 found that the embedment length plays a dominant role on the behaviour of fibre pull-out as a short embedment length at inclination angle of 30° degrees for ultra-high-performance concrete caused matrix fracture failure. Robins *et al.* 46 also suggested that unless embedment length is higher than the hooked-end length, the pull-out load is reduced. Abdallah *et al.* 49 concluded that the embedment length had no influence on the pull-out strength but merely increased the slip and ductility. Hence, it is important to investigate the effect of L_E on SFRLC. For instance, although 30 mm embedment length maximises the frictional fibre pull-out for 3D fibres used (d_f = 60 mm), it is thought that an embedment length L_E = 30 mm can lead to an unrealistically favourable case of uniaxial tensile tests, as in a real structural member cracking can manifest anywhere along the fibre and is more likely to occur at a shorter embedment length. Thus, the embedment length was initially fixed at 30 mm, 20 mm and 10 mm for different specimens based on a crack that is expected to take place in the middle of the 10 mm notch.

An angle of 0° to the load is considered as the most unfavourable in a hooked-end fibre pull-out test due to the lowest possible frictional resistance and the shortest required length for fibre straightening (only hooks will be straightened) before being pulled-out. Consequently, the fibre stress developed during pull-out will be lower than the maximum stress capacity of the fibre. If the angle was too large, concrete matrix fracture failure could also develop due to the matrix spalling caused by the snubbing effect along the bent part of the steel fibre 55. Depending on fibre tensile strength, in theory as the angle to the load is increased, frictional resistance is increased which resulted in an increase in uniaxial tensile strength of SFRLC until reaching the maximum tensile strength of fibre leading to rupture, so long as the concrete matrix does not break due to the concentrated normal force from the fibre and given that the embedment length does not reduce to the point where the hook is not well bonded. Recent research on ultra-high-strength concrete by Cao and Yu 55 revealed that the inclination angle for maximum pull-out load can be around 20°-30° to the horizontal (and 10°-20° for Robins *et al.* 46), provided that fibre tensile strength is high enough to prevent fibre rupture and the matrix is strong and dense enough to prevent matrix fracture. Since the lightweight concrete used is not as dense as ultra-high-strength or normal weight concrete and that LWAC is known to have air pores, and for design purposes 56, it was decided that an angle of 0° was to be adopted as the base for design in the pull-out tests, while a few specimens with other angles were tested for completeness.

Finally, the aspect ratio which is defined as L_f/d_f can also impact the pull-out behaviour. It was found that the longer the fibre, the more efficient the crack bridging 43. Based on all the above observations, the testing programme comprised an extensive fibre pull-out investigation which considered the following parameters: V_f = 0, 1 and 2%, f_{lck} = 30, 35 and 40 MPa, L_f/d_f = 65 and 80, d_f = 0.55, 0.75 and 0.9 mm, L_f = 35 and 60 mm, number of fibre hooks or bends n_b = 1(3D), 2(4D) and 3(5D), and inclination angles of 20° and 45°. Also, 3D and 5D fibres with hooks being cut off were tested to check the viability of mixing straight fibres of different tensile strengths with lightweight concrete and to quantify the contribution of the hooks on the pull-out behaviour.

4. Results and Discussion

The workability, density and uniaxial compressive cube strength results were detailed in an accompanying paper for mixes 1-3D, 1-4D, 2 and 3 [30,31]. The additional mixes 1-3D* and 1-3D** showed similar workability, density properties and compressive strength results to mix 1-3D and these results are summarised in **Error! Reference source not found.** (data for convenience mixes 1-3 also included). To avoid repetition, the interpretation of the results and trends can be directly adopted from the accompanying paper [30,31]. In summary, it was found that the mechanical properties were improved with the addition of fibres, and the density was largely unaffected, which is important for LWAC applications. On the other hand, the workability was significantly reduced with the

Commented [M1]: Please check if this should be Table 3.

Commented [AA2R1]: Corrected to Table 3.

addition of more than 2% volume fraction of fibres. This further emphasises that for fibrous mixes, fibre dosage should not exceed V_f = 1.5 - 2% based on workability challenges if no superplasticisers or water reducing agents are used. It also appears that the mixes having fibres with more extensive hooks held the slump together more tightly which led to lower slump values than those mixes having fibres with less extensive hooks. It should be noted that mix 1-3D** with the shortest fibres 3D** exhibited the highest slumps and highest densities amongst all mixes.

Table 3. Mean values of Slump, water saturated density (oven dry density with *), cube compressive strength average values for mixes 1-3. *Standard Deviation between brackets*.

Mix	**f_{lck} (MPa)**	**Fibre**	**Slump (mm)**			**Density (kg/m³)**			**$f_{lcm,cube}$ (MPa)**		
			Plain	**V_f = 1%**	**V_f = 2%**	**Plain**	**V_f = 1%**	**V_f = 2%**	**Plain**	**V_f = 1%**	**V_f = 2%**
1-3D	30	3D	91 (7.6)	66 (3.1)	32 (5.2)	1981 (124) *1723 (159)	1992 (182)	1979(133)	37 (3.1)	37 (4.1)	38 (3.2)
1-3D*	30	3D*	96 (8.1)	57 (3.1)	31 (2.8)	1968 (144) *1693(163)	1963 (161)	1979(189)	39 (2.2)	41 (3.8)	40 (3.1)
1-3D**	30	3D**	103 (10.2)	87 (4.4)	42 (4.6)	2001 (137) *1731(122)	1991 (149)	1986(173)	37 (5.1)	38 (2.9)	37 (6.3)
1-4D	30	4D	98 (11.2)	49 (3.3)	26 (4.1)	1998 (166) *1777 (172)	1962 (171)	1951(111)	36 (4.3)	37 (3.8)	34 (4.2)
2	35	3D	86 (7.2)	46 (6.1)	28 (2.1)	2000 (178) *1786 (153)	1988 (182)	1963(121)	45 (5.6)	42 (3.8)	44 (3.2)
3	40	5D	88 (4.9)	42 (1.3)	20 (2.6)	1954 (121) *1712 (142)	1936 (168)	1917(167)	50 (6.8)	49 (4.2)	51 (3.1)

4.1. Pull-Out Load-Slip Behaviour

A fully straightened hooked-end 3D fibre photographed at the end of testing is shown in **Error! Reference source not found.**. It can be seen that the effective cylinder through which the fibre was embedded contained aggregates as well as cement and sand at the notch through which the fibre was centred. This proves that the mould used, and the testing design adopted, were adequate at mimicking the realistic behaviour of SFRLC at the crack.

Figure 6. Pull-out specimen at the end of testing.

Error! Reference source not found. depicts the pull-out load-slip behaviour of some key specimens tested (with the salient features summarised in **Error! Reference source not found.**). Overall, the behaviour of SFRLC specimens in pull-out can be summarised in the following stages. Initially, an elastic stage takes place until the point of cracking. This point approximately coincides with the load at which *plain* concrete would fail in uniaxial tension and is roughly the case for all the specimens tested of similar concrete grade regardless of the type of fibre or fibre volume fraction. This shows that the fibres have insignificant effect on the elastic uniaxial tensile behaviour of SFRLC and only become active once concrete cracks. In the absence of any innate tension stiffening mechanism such as in the case of brittle plain lightweight concrete, a sudden drop in load to 0 is seen (which is the case for the plain concrete specimen, i.e. V_f = 0%, in **Error! Reference source not found.**).

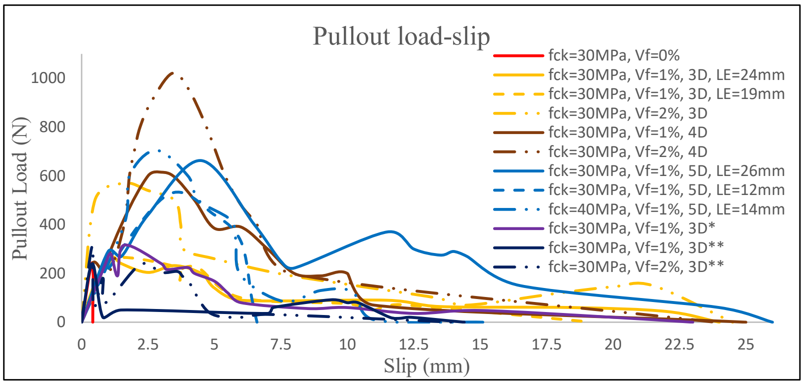

Figure 7. Mean pull-out load-slip behaviour of key specimens tested.

With the incorporation of steel fibres however, the plain lightweight concrete peak tensile strength where the principal crack is fully formed is followed by a drop then increase in load. This behaviour largely agrees with uniaxial tensile tests on SFRC carried out by Barragán *et al.* 57 and Abdallah *et al.* 43 and pull-out tests by Robins *et al.* 46. This marks the fibre bridging phase, which is initially characterised by an elastic behaviour followed by fibre debonding where gradual loss of frictional bond between the fibre and matrix is seen. Afterwards, the activation of mechanical hooking is initiated. This behaviour was also reported by Qi *et al.* 56. This results in an increase in the peak residual tensile load due to fibre reinforcement only. This load is mainly affected by concrete strength, fibre mechanical anchorage (number of hooks), fibre diameter, fibre tensile strength and inclination angle. Also, if the embedment length is not adequate to cater for hook straightening and thus mobilisation of the maximum possible fibre stress for the composite, the peak load can be reduced drastically due to the possibility of matrix cracking at hook ends. Maintaining this load solely relies on the bond between the steel fibres and concrete. During this stage, the fibre undergoes plastic deformation at hooks and plastic hinges are developed. The maximum number of plastic hinges at the maximum load become active (2 for 3D, 3 for 4D and 4 for 5D). This stage is followed by stress relaxation which is characterised by full hook straightening and deactivation of plastic hinges. Finally, frictional fibre-matrix pull-out occurs and the test ends with the fibre being completely pulled out.

Table 4. Average deformation histories of uniaxial tensile pull-out test. [1] fibre at angle 20°; [2] fibre at angle 45°; [3] concrete fractured; [4] hook-less 5D fibre; [5] hook-less 3D fibre; [6] slip at maximum pullout; [7] ultimate slip where fibre has pulled-out.

f_{lcm} (MPa)	V_f (%)	Fibre type	L_E (mm)	P_{max} (N)	Δ_{max}[6] (mm)	Contribution of fibre [interval] (mm)		Δ_u[7] (mm)
						Hook	Pull-out	
30.1	0			244	0.8			0.8
36.5	0			267	0.73			0.73
44.1	0			320	0.68			0.68
33.3	1	3D	18.41	265	1.6	[1, 6]	[6, 19.2]	19.2
32.8	1	3D	23.5	266	1.2	[0.6, 6.6]	[6.6, 24]	24
35.0	2	3D	24	570	1.6			24.5
34.9	1	4D	24.4	615	3.1	[0.6, 9.3]	[9.3, 25]	25
34.6	2	4D	23.4	1020	3.4			23.8
34.3	1	4D[1]	18.7	625	6	[0.42, 9.2]	[9.2, 19.1]	19.1
34.1	1	4D[2]	19	690	8.1	[1.1, 8.1]		8.1
36.2	1	3D	12.9	326	1.8	[1.4, 6.4]	[6.4, 13.9]	13.9
34.6	1	5D	25	662	4.5	[2.5, 12.5]	[12.5, 26]	26
44.1	1	5D	14.45	705	2.8	[1.1, 11.1]	[11.1, 15.1]	15
44.1	1	5D[3]	11	520	3.2	[1, 5]		12
31.5	0.7	3D*	21.7	316	1.6	[1.35, 6.3]	[6.3, 23]	23
31.0	0.4	3D**	14	92	9.4	[7.2, 12.4]	[12.4, 14.4]	14.4
38.2	1.2	3D**	13.6	236	2.2			14
32.4	1	5D[4]	14.8	30-56	1.2		[0.4, 15.2]	15.2
32.4	1	3D[5]	20.8	34-52	0.42		[0.4, 23]	21.4

4.1.1. Effect of Number of Bends n_b

To investigate the effect of the number of fibre bends or hooks, specimens with 3D, 4D and 5D fibres with V_f = 1% were all compared. All fibres had an embedded length of approximately L_E = 25 mm (which was established before the test), an identical aspect ratio L_f/d_f = 65 and similar compressive strengths. A maximum pull-out strength of P_{max} = 267 N was recorded for the 3D sample while P_{max} = 615 N and P_{max} = 662 N were recorded for both 4D and 5D samples, respectively. Although not only the number of bends differed between the 3 fibres but also the maximum fibre tensile strength, the 3D and 4D samples failed after complete straightening of bends while 5D samples showed partial straightening of bends, then all fibres pulled out without fibre rupture taking place. This suggests that the number of bends or hooks is the most influential factor in the behaviour of fibrous lightweight concrete (with the same fibre aspect ratio, and shows that a higher number of bends or hooks may lead to higher pull-out strength since more plastic hinges are developed and more bend straightening is required due to developing a better concrete-fibre bond. Also, it can be observed that the post-cracking ductility increases with the increase of the number of bends, as the load can be maintained at a high stress level for a longer duration of the test. It should be reminded however that most 5D hooks appeared to not be straightened completely after pull-out (**Error! Reference source not found.**). The reasons behind partial hook straightening of 5D fibre will be further investigated in 0.

Figure 8. 5D hook not fully straightened following the pull-out test.

4.1.2. Effect of Fibre Aspect Ratio a_f

To investigate the effect of fibre aspect ratio a_f (defined as L_f/d_f), the 3D* fibre with a_f = 80 (L_f = 60 mm, d_f = 0.75 mm) was tested. The 3D* fibre had nearly identical properties including the maximum fibre tensile strength, length and geometrical hooks to those of the control 3D fibre with a_f = 65 (L_f = 60 mm, d_f = 0.9 mm). However, the 3D* fibre developed a maximum pull-out strength of P = 316 N which is 15% higher than that of the control 3D fibre. This shows that a higher aspect ratio leads to developing a higher tensile strength.

4.1.3. Effect of Fibre Length L_f

To study the effect of fibre length, 3D** fibre with aspect ratio a_f = 65 (L_f = 35 mm, d_f = 0.55 mm) was tested. The 3D** fibre has an almost identical hook length to 3D fibre and a slightly higher maximum fibre tensile strength. This fibre proved to be somewhat the weakest as it generated a pull-out force of only P = 92 N. Hence, the longer the fibre the more efficient the crack arresting mechanism. This agrees well with Abdallah *et al.* 43 findings.

4.1.4. Effect of Fibre Dosage V_f

To study the effect of increasing fibre dosage, mixes of similar fibre types are compared for different fibre volume fraction V_f = 1% and 2%. For 3D fibres, the pull-out strength was recorded to be P = 570 N at V_f = 2% which is 53% higher than the corresponding pull-out strength at V_f = 1%. Whereas, for 4D and 5D fibres the increase in strength (when V_f was raised from 1% to 2%) was calculated to be 44% and 50%, respectively. This enhancement was expected since the fibre dosage was doubled.

4.1.5. Effect of Compressive Strength f_{ck}

To examine the effect of lowering the concrete grade, specimens with compressive strength f_{ck} = 40 MPa reinforced with 5D fibres were tested. When their pull-out behaviour was compared to that for concrete specimens with f_{ck} = 30 MPa (also reinforced with 5D fibres), the pull-out tensile strength developed was 7% higher for the higher concrete grade. Hence, increasing the concrete grade by increasing cement content and reducing w/c ratio leads to a reduction in air pores around the embedded hooks, which increases the mechanical bond strength. This behaviour is also reported by Abdallah *et al.* 49.

4.1.6. Effect of Embedded Length L_E

To examine the effect of varying the embedment length L_E on the tensile strength, mixes sharing the same properties (f_{ck} = 30 MPa, V_f = 1%, 3D) but with different embedded lengths ($L_{E,1}$ = 18.4 mm and $L_{E,2}$ = 23.5 mm) were compared. For both specimens, a similar pull-out load P_{max} ≈ 265 N was measured, albeit the specimen with higher embedded length provided higher ductility. The latter will be inspected by calculating Pull-out work done in Section 0. It is interesting to observe that some specimens experienced concrete fracture then pull-out at the hook's location such as the specimen with properties: f_{lck} = 30 MPa, V_f = 1%, 5D. **Error! Reference source not found.** shows a concrete specimen fracturing outside the notch. For this particular sample, the embedded length was only 12 mm while the hook length is approximately 10.1 mm for 5D fibres. Therefore, the embedment length L_E was deemed insufficient. Another identical specimen with L_E = 14.45 mm was seen to be capable of undergoing the complete hook straightening before being pulled-out. Therefore, altering the embedment length of the hooked-end fibres for lightweight concrete has no practical effect on the maximum pull-out strength, but merely increases the ductility via frictional pull-out as long as L_E provides enough hook bond (i.e. when L_E ~ L_h + 4.5 mm with L_h being the hook length). This phenomenon was also observed with 3D and 4D fibres. Hence, if the fibre diameter d_f is to be factored into the previous equation, then $L_E = L_e \sim L_h + 5d_f$, with L_e as the length required to develop the maximum pull-out strength of fibre based on pull-out tests. This finding also agrees with Abdallah *et al.* 49 observations, who recommended $L_E = L_h$ + 5 mm for developing maximum pull-out load P_{max}.

Figure 9. Concrete fracture outside the notch.

4.1.7. Effect of Fibre Inclination Angle θ_f

To study the effect of the orientation angle which is the angle between the tensile load applied and the fibre, 4D fibres at angles 20° and 45° were tested and plotted (**Error! Reference source not found.**). It can be seen that the specimen whose fibre was oriented at 45° failed in concrete fracture similar to the specimens with inadequate embedded length, although it developed a higher pull-out tensile strength of P = 690 N than its counterparts. By contrast, a pull-out strength of only P = 626 N was recorded for the specimen with an orientation angle of 20°. However, the latter failed in a ductile fibre pull-out mode. This pull-out strength is 11 N higher than that developed by the control specimen of f_{lck} = 30 MPa, V_f = 1% and fibre 4D with an orientation angle of 0°. Hence, it can be deduced that by increasing the orientation angle, the load increases and takes place at a larger slip. If the angle is too high and the concrete is not dense enough, the concrete can fracture and fail in a brittle manner. These findings agree with Robins *et al.* 46 study, with the exception that the fibres used in that work ruptured at a higher inclination angle. However, in the present work the concrete fractured. This could be attributed to the enhanced tensile strength of the 4D fibres as compared to the fibres mixed in the experiments carried out by Robins *et al.* 46 coupled with the porous nature of LWAC which could induce cracking and fracturing much more readily.

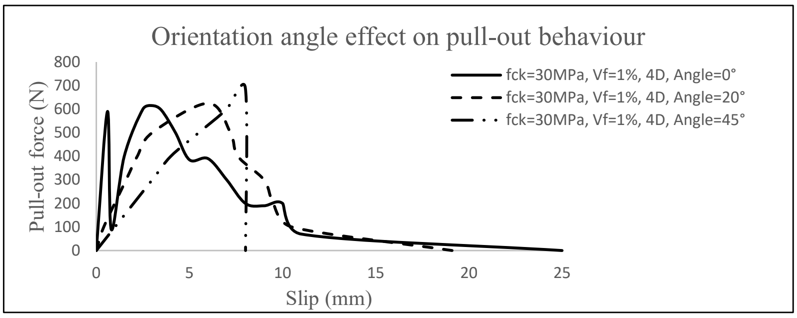

Figure 10. Pull-out load-slip behaviour with different orientation angles for 4D specimens.

It is important to note that for some specimens such as the one showed in **Error! Reference source not found.** with orientation angle 0°, the load increased to an unexpected value (in this example 590 N) before any activation of fibre pull-out. This value is thought to be overly high for concrete in tension of f_{lck} = 30 MPa which usually was of pull-out strength P_{max} = 244 N. Upon inspection of the pulled-out specimen after the test, it was observed that a lightweight aggregate positioned at the notch was split which led to a drastic increase in the load. It was also interesting to measure that the aggregate had a diameter of almost 5 mm (**Error! Reference source not found.**), i.e. 7 mm smaller than that of the notch, which should not force the crack to go through it. However, this can be justified, since for other material tests such as compression tests - detailed in the earlier paper [30,31], some of the aggregates were sheared through in a similar manner. In the same test, this was followed by a sudden drop of load before fibre activation took place.

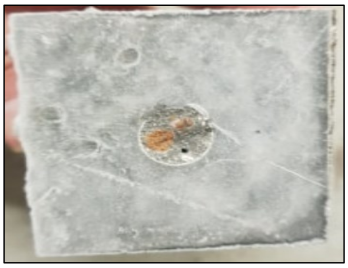

Figure 11. A pull-out specimen with a split 5 mm aggregate at the notch.

4.1.8. Adequacy of Smooth Fibres

In order to investigate the possibility of mixing lightweight concrete with straight smooth round fibres, 3D and 5D fibres with hooks being cut off were tested, with the ensuing results depicted in **Error! Reference source not found.**. The difference in embedded length is due to the longer 5D hooks (about 10 mm for each hook which resulted in 40 mm fibre remaining straight length), compared to the 3D hooks (about 5 mm for each hook which resulted in a 50 mm fibre length). For both fibres, the load dropped right after cracking at about 35-50 N and a decay curve ensued with hardly any upgrade in load. These values agree with Alwan *et al.* 47 pull-out loads from tests with shorter straight and smooth DRAMIX fibres embedded in concretes with low strengths. Also, Abdallah and Rees 58 tested straight DRAMIX fibres embedded in concrete with compressive strength of 33 MPa and recorded similar values. The present tests demonstrate the importance of hooks in the structural responses of fibrous lightweight concrete, since the hook-less 5D and 3D fibres only maintained the load until the eventual pull-out. Thus, it can be concluded that the usage of straight fibres is not recommended for lightweight concrete due to its low densification, resulting in a weak fibre-matrix interfacial bond strength which causes the smooth straight fibres to pull-out easily.

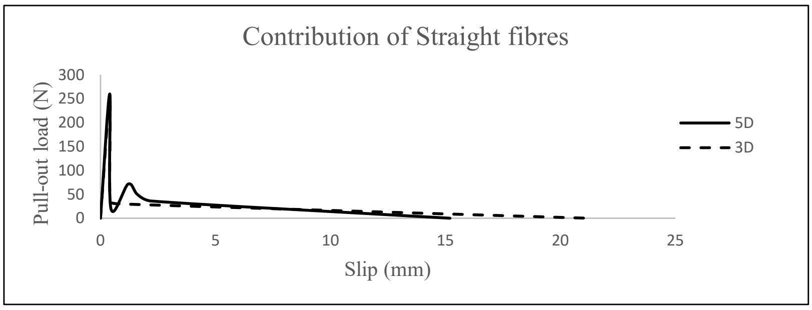

Figure 12. Pull-out load-slip behaviour of straight fibres.

It is important to note that for all the preceding specimens examined according to the pull-out test, any observed upgrade in the uniaxial tensile or pull-out strength (due to the addition of fibres) might not occur in a different structural element where fewer fibres than those designed for were *actually* present in the vicinity of the crack. Other reasons related to insufficient embedded length and unfavourable fibre orientation angle (for example vertical to the tensile load or that which causes concrete fracture above 45°-50°). All these reasons can lead to lowering the uniaxial tensile strength developed due to fibre reinforcement. By contrast, a favourable inclination angle (about 20°) and an optimum embedment length ($L_E = L_f/2$) would enhance the pull-out behaviour and energy dissipation. For this reason, fibre orientation factor η will be discussed later on to examine its effect on the post-cracking uniaxial tensile stress.

4.2. Key Characteristics of the Uniaxial Tensile Behaviour of SFRLC

Error! Reference source not found. summarises the key parameters defining the uniaxial tensile behaviour of fibrous composite. Each of these parameters will be discussed next.

Table 5. Assessment of the pull-out behaviour.[1] maximum tensile stress unfactored (orientation factor (η_0) = 1) of plain or fibrous concrete; [2] work done; [3] average bond stress; [4] equivalent bond stress; [5] ultimate bond stress;[6] fibre efficiency. *Standard deviation for f_{lcm} and $f_{lctm,m}$ between brackets*.

f_{lcm} (MPa)	V_f %	Fibre type	$f_{lctm,m}$[1] (MPa)	W_{total}[2] (N.mm)	τ_{av}[3] (MPa)	τ_{eq}[4] (MPa)	τ_{ult}[5] (MPa)	ξ[6]
30.1 (3.8)	0		2.16 (0.13)					
36.5 (4.2)	0		2.36 (0.17)					
44.1 (5.7)	0		2.83 (0.37)					
33.3 (4.1)	1	3D	4.17 (0.39)	1801.6	5.1	3.8	9.83	0.36

32.8 (3.3)	1	3D	4.18 (0.41)	2167.8	4.01	2.8	9.85	0.36
35.0 (4.4)	2	3D	8.96 (0.72)	4655.1				
34.9 (4.1)	1	4D	9.67 (1.02)	4085.8	8.9	4.9	16.6	0.65
34.6 (3.2)	2	4D	16.03 (1.38)	6073				
34.3 (4.7)	1	4D	9.82 (1.11)	4547.5				0.65
34.1 (4.1)	1	4D	10.85 (0.82)	2898.5				0.72
36.2 (6.2)	1	3D	5.12 (0.35)	1551.2	6.93	6.6	12.1	0.44
34.6 (4.9)	1	5D	10.41 (1.33)	6170.5	9.37	7	16.1	0.45
44.1 (5.9)	1	5D	8.17 (0.37)	2216				0.36
44.1 (6.7)	1	5D	11.08 (1.21)	3257.8	17.3	11.04	17.1	0.48
31.5 (2.1)	0.7	3D*	5.01 (0.59)	1812.8	6.2	3.3	15.2	0.58
31.0 (8.1)	0.4	3D**	1.55 (0.13)	667.8	3.8	3.9	6.8	0.29
38.2 (4.9)	1.2	3D**	3.97 (0.41)	903.7				
32.4 (2.1)	1	5D	0.49 (0.08)	325	1.7	1.05	1.26	0.08
32.4 (6.2)	1	3D	0.53 (0.04)	318	0.6	0.5	0.48	0.04

4.2.1. Maximum Uniaxial Tensile Stress $f_{lctm,m}$

The maximum uniaxial tensile stress $f_{lctm,m}$ is the larger of the uniaxial tensile stress due to plain concrete $f_{lctm,p}$ or the post-cracking residual tensile stress due to fibre concrete $f_{lctm,f1}$. $f_{lctm,p}$ can be calculated using the pull-out response by dividing P_{max} for plain specimens by the area of the notch. To calculate the contribution of steel fibres to the tensile strength of concrete at any instant, the rule of composites is used. Thus, the actual composite stress is:

$$f_{lctm,fi} = \sigma_{av,f} + \sigma_c \quad (1)$$

$\sigma_{av,f}$ and σ_c are the average stresses of fibre and concrete, respectively.

From 59,27,60,61, the fibre contribution can be calculated using the following expression:

$$\sigma_{av,f} = \sigma_f V_f \eta_0 \quad (2)$$

where V_f is the fibre volume fraction and η_0 is the fibre orientation factor taken as 0.41.

Hence, Eq. (1) becomes:

$$f_{lctm,fi} = \sigma_f V_f \eta_0 + \sigma_c (1 - V_f) \quad (3)$$

The classical contribution of both concrete and steel fibres in a SFRC composite remains true for SFRLC with $\sigma_f \approx 0$ before cracking and $\sigma_c = 0$ after cracking, since it was demonstrated from the experiments that practically only steel fibre reinforcement contributes to tension stiffening for lightweight concrete immediately after matrix cracking. Following cracking, once the maximum pull-out strength P_{max} for a single fibre is known, fibre stress σ_f can be readily derived using: P_{max}/A_f with A_f as the area of a single fibre. Hence, at post-peak, the maximum residual stress (or first residual stress $f_{lctm,f1}$) of SFRLC can be calculated using the following equation:

$$f_{lctm,f1} = \sigma_f(\text{peak}) V_f \eta_0 = P_{max}/A_c \, V_f \eta_0 \quad (4)$$

$f_{lctm,m}$ is increased by the addition of fibres, increase in V_f and the number of bends. It should be noted that the post-cracking residual tensile stress $f_{lctm,f1}$ used to derive $f_{lctm,m}$ for fibrous specimens in **Error! Reference source not found.** is unfactored. To account for the random distribution of fibres in a 3D real fibrous concrete structural element, an orientation factor is introduced as $\eta_0 = 0.41$ (27). The orientation factor can be defined differently in the literature ($\eta_0 = 0.5$ 62 and variable according to size effect 63).

Fig 13 shows the uniaxial tensile strength $f_{lctm,f1}$ of the SFRLC specimens tested, normalised to the corresponding plain concrete strength of the same grade $f_{lctm,p}$. From **Error! Reference source not found.**, the maximum SFRLC post-cracking residual uniaxial tensile strength $f_{lctm,f1}$ reinforced with $V_f = 1\%$ was 54%, 126%, 135%, 92%, 46%, 7% and 15% of plain concrete strength of the same grade $f_{lctm,p}$ when fibres of 3D, 4D, 5D, 3D**, 3D*, hook-less 3D and hook-less 5D, were added, respectively. This discrepancy in enhancing the residual fibrous tensile resistance of SFRLC between these mixes was essentially emanated from the effectiveness of bond between concrete and steel fibres. Using **Error! Reference source not found.**, it can be seen that with the addition of $V_f = 1\%$, all fibres showed a residual tension softening behaviour with the exception of 4D and 5D fibres, which exhibited a residual tension hardening behaviour. However, with the increase of V_f to 2%, 3D fibres were also able to induce a tension hardening effect based on $f_{lctm,m}/f_{lctm,p}$ ratio being larger than 1.

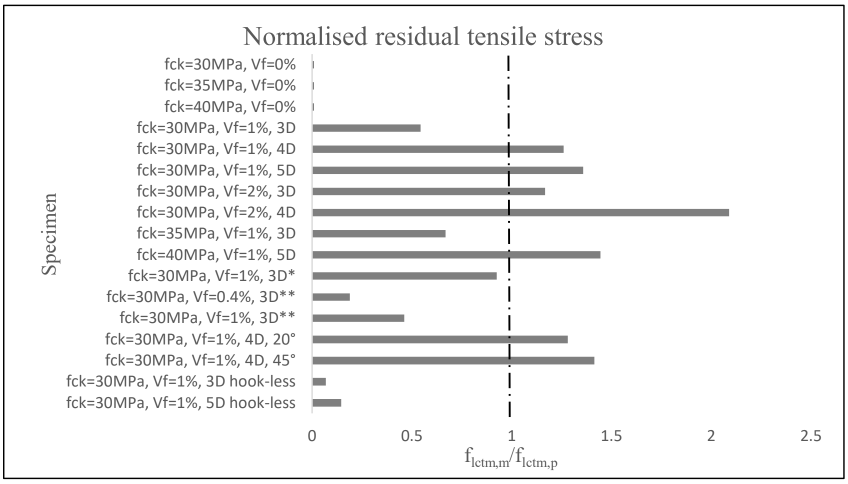

Figure 13. Normalised uniaxial tensile stress of the specimens tested.

4.2.2. Pull-Out Work

Work done is a measurement of ductility and is estimated by calculating the area under the pull-out load-slip curve. The work done is governed by three parameters, the fibre type, fibre volume fraction and embedment length. From **Error! Reference source not found.**, it appears that the fibre type is the most influential of the three parameters. For instance, 5D fibres with $V_f = 1\%$ brought about a higher total work than 4D fibres with $V_f = 2\%$ for similar L_E and concrete strength. Hence, 5D fibres are seen to provide the highest work done followed by 4D, 3D, 3D* then 3D**. Also, the higher the volume fraction V_f, the higher the total work done. Moreover, clearly the larger L_E, the more the energy dissipation through fibre frictional pull-out, which in turn translates to a more ductile response of the pull-out load-slip curve.

4.2.3. Bond Strength

Several equations were developed in the past to quantify and assess the bond behaviour between fibres and concrete. The most important of which were summarised in **Error!**

Reference source not found.. The average bond stress τ_{av} 54 is defined as the maximum pull-out strength divided by the initial bond area between concrete and embedded fibre:

$$\tau_{av} = P_{max}/\pi d_f L_E \quad (5)$$

where τ_{av} (MPa) is the average fibre-matrix interfacial bond shear stress, d_f (mm) is the fibre diameter and L_E (mm) is the initial embedment length defined as the shorter length of the embedded fibre after the crack takes place at the notch in the pull-out specimen. Since the experiments conducted showed that the embedment length plays no practical role in altering the maximum pull-out strength, but merely affects the frictional pull-out, the average bond strength gives a poor estimate of bond if the latter is to be directly linked to the peak strength. The equivalent bond strength τ_{eq} 64 is defined as the fibre-matrix interfacial bond stress during the entire fibre pulling-out process using the total work due to fibre pull-out:

$$\tau_{eq} = 2W_p/\pi d_f L_E^2 \quad (6)$$

where W_P (N.mm) is the total work done by fibre, which is equivalent to the area under the stress-slip once concrete cracking develops. The equivalent bond strength governs how effective is the concrete crack control and therefore can be regarded as a direct measure of evaluating the structural performance including ductility and ultimate loading capacity of fibrous concrete. Since P_{max} is affected only by the fibre hook contribution, then the embedded length must be at least $L_E = L_e = L_h + 5d_f$ for complete fibre hook straightening. It should be reminded that a higher value of the embedded length $L_E > L_e = L_h + 5d_f$ will not increase the pull-out strength as shown previously. Eq. (4) is rearranged to become:

$$P_{max} = \tau_{ult}\pi d_f(L_h + 5d_f) \quad (7)$$

Hence, the ultimate bond strength of the SFRLC composite with hooked-end fibres can be written as:

$$\tau_{ult} = P_{max}/\pi d_f(L_h + 5d_f) \quad (8)$$

The ultimate bond strength for the fibres mixed with different lightweight concrete grades are summarised in **Error! Reference source not found.**. It should be noted that for the hook-less 3D and 5D fibres, L_h was taken as the total embedded length.

It can be seen from the experimental data that 4D fibres resulted in the highest ultimate bond strength therefore exceeding both 3D and 5D ultimate bond strengths for the same concrete grade of f_{lck} = 30 MPa. On the other hand, 3D** developed the lowest bond strength amongst hooked-end fibres. Also, it should be noted that by increasing the concrete grade, the ultimate bond strength increased as well. This was seen for 5D and 3D specimens tested with f_{lck} = 30 and 40 MPa. In addition, 3D* fibres with L_f/d_f = 80 aspect ratio developed an average bond strength 55% higher than that of 3D fibres with L_f/d_f = 65. Hence, for DRAMIX hooked-end fibres, the high aspect ratio brings about a higher bond strength. Lastly, the lowest bond strength was calculated for the smooth straight fibres (i.e. hook-less fibres).

4.3. Fibre Optimisation

In order to determine the fibres that are best suited for reinforcing the lightweight concrete tested, a brief optimisation study is carried out as discussed next.

4.3.1. Fibre Stress Efficiency

Fibre stress efficiency values are summarised in **Error! Reference source not found.**. Fibre efficiency is a direct measure of the effectiveness of fibre reinforcement for a particular concrete. A very low value indicates an under-performance of fibre reinforcement while a very high value may indicate over-performance of fibre reinforcement which may lead to fibre rupture. Also, fibre efficiency can be a direct measure for the calculation of the formation of plastic hinges and straightening of fibres. Fibre stress efficiency ξ is calculated by dividing the maximum stress by the ultimate stress of fibre. Amongst all the fibres tested, 4D and 3D* fibres showed the highest fibre stress efficiency, followed by 5D, 3D, 3D** and lastly hook-less 3D and 5D. Since 3D, 3D* and 3D** fibres have roughly identical hook shape and size, the higher aspect ratio and fibre length are therefore the most responsible parameters for developing fibre stress efficiency given that concrete strength is kept constant. Increasing the inclination angle led to a greater fibre efficiency as seen with 4D fibres, however this could cause concrete fracture for the porous light-weight concrete matrix. A higher concrete grade which means a lower w/c ratio and a denser concrete matrix would bring about a better bond, which in turn would result in a higher fibre stress efficiency. Lastly, L_E played no factor in increasing fibre stress efficiency.

4.3.2. Fibre Energy and Bond Indices

In order to further investigate the behaviour of SFRLC for fibre optimisation, assessment of energy dissipation and bond strength is vital. Qi *et al.* 56 aimed to choose the fibre type best suitable for the concrete tested by defining both the energy dissipation index η_f and bond strength index ζ_f using a single fibre pull-out test.

$$\eta_f = W_p/A_f L_f \quad (9)$$

$$\zeta_f = \tau_{av}/A_f L_f \quad (10)$$

However, these two equations need adjustment of the accuracy of their mechanical meaning based on the pull-out tests carried out previously. This is the case because it was shown that the fibre length L_f plays no role in enhancing bond strength and minimal role in energy dissipation when compared to L_E. Therefore, Eq. (9) and (10) become:

$$\eta_{f,actual} = W_p/A_f L_E \quad (11)$$

$$\zeta_{f,actual} = \tau_{ult}/A_f(L_h + 5d_f) \quad (12)$$

Error! Reference source not found. shows the normalised actual efficiency indices which are calculated by dividing the actual efficiency indices by the control 3D specimen actual efficiency indices. It can be seen that the more extensive the hooks, the higher the energy dissipation efficiency index. Consequently, 5D and 4D fibres recorded the highest energy efficiency indices due to the longer hooks which increase energy dissipation. Also, the higher the aspect ratio for similar fibre length, the higher the energy dissipation efficiency index as can be seen with 3D* (a_f = 80) as compared to 3D and 3D** fibres which have a similar aspect ratio (a_f = 65). Fibre bond strength efficiency index varies, with 3D* having the highest and 3D and 5D fibres recording the lowest values.

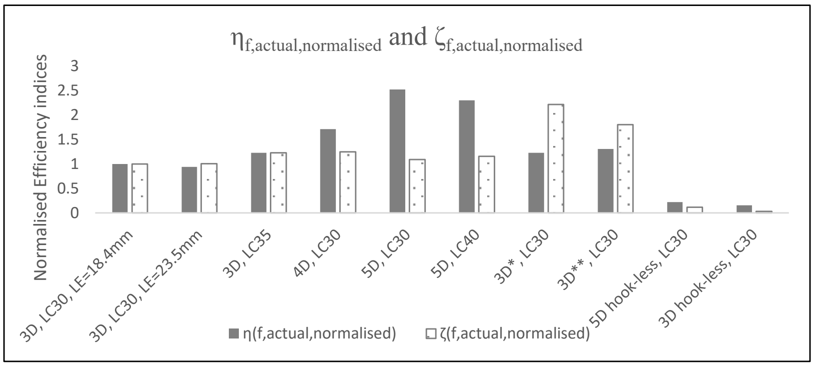

Figure 14. Normalised actual efficiency indices for the pull-out specimens tested.

4.3.3. Fibre Plasticity Study

As shown previously in **Error! Reference source not found.**, all fibres appeared to be straightened then pulled-out of the lightweight concrete notched prisms with the exception of some 5D specimens. When the 5D fibres were not fully straightened, a local fracturing of matrix followed, which is an unfavourable mode of failure. Not becoming fully straightened translates into lack of developing full plastic hinges, which is why 5D fibre stress efficiency was low. To this end, fibre tensile stress was thought to play a secondary role in the behaviour of the pull-out specimens, however the high yield stress of 5D fibres combined with the hook geometry and angles (summarised in **Error! Reference source not found.**) are thought to play a negative role in preventing steel yielding of fibre and thus increase the possibility of fracture. To investigate the latter, Alwan *et al.* 47 pulley model, depicted in Fig 15, is adopted to determine the magnitude of the load causing the plastic hinges to form preceding hook straightening. This theoretical pull-out load was then compared to the corresponding experimental one.

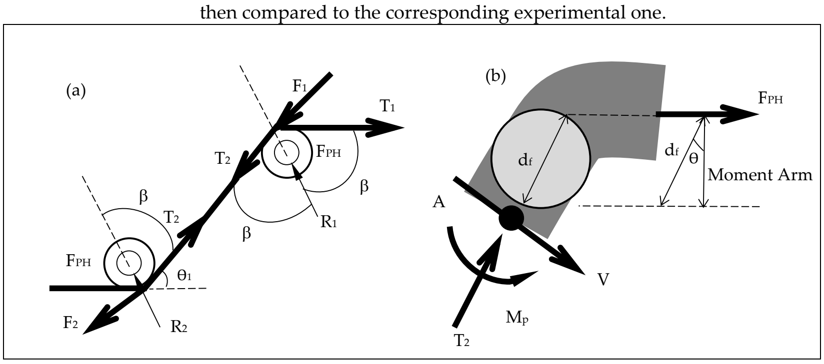

Figure 15. a- Pulley model for 3D fibres and b- FBD for a plastic hinge at a fibre hook (adapted from 47 and 48).

In **Error! Reference source not found.**, F_{PH} corresponds to the cold work needed to straighten the steel fibre at the location of plastic hinge, M_P is the plastic moment of the steel fibre and T_2 is the chord tension in the fibre. Since the purpose of this section is to determine the force required to develop plastic hinge and straighten the fibre, F_{PH} was calculated for 3D, 4D and 5D fibres.

Taking moments about point A.

$$F_{PH} = M_p/d_f\cos\theta \qquad (13)$$

The plastic moment M_P is suggested from Alwan *et al.* 47 who carried out pull-out experiments of 3D DRAMIX fibres embedded in concrete of w/c ratios ranging from 0.5 to 1.0. In Alwan *et al.* study 47, the pull-out loads were of around 150-180 N for 3D fibres whose aspect ratio was 0.6 (d_f = 0.5 mm, L_f = 30 mm) which are comparatively higher than the pull-out loads recorded in this work for 3D** fibre with d_f = 0.55 mm and L_f = 35 mm, whose pull-out loads were around 90-105 N. The plastic moment from 47 is:

$$M_P = f_y \cdot \pi r_f^2/2 \cdot d_f/3 \qquad (14)$$

with r_f as the radius of the fibre. It should be noted that Eq. (14) was thought to be suitable for concretes where an elastic-plastic condition is sufficient for fibre pull-out. Abdallah *et al.* 48 suggested the following plastic moment and criticized that Eq. (14) underestimates the pull-out for ultra-high strength concrete:

$$M_P = f_y \cdot \pi r_f^2/2 \cdot d_f/3 \cdot \pi/4 \qquad (15)$$

Based on Alwan *et al.* 47 theoretical hooked-end 3D fibre pull-out depicted in **Error! Reference source not found.** (which agrees with the current experimental study), the maximum pull-out load is:

$$P_{max} = P_2 = P_1 + \Delta P' = P_1 + T_1 \qquad (16)$$

where $\Delta P'$ or T_1 is the contribution of plastic hinges to pull-out load and P_1 is the pull-out load at the onset of complete debonding. P_{max} or P_2 can be found from **Error! Reference source not found.**. The total number of possible plastic hinges is 2, 3 and 4 for 3D, 4D and 5D fibres, respectively. Since hooked-end and straight fibres pull-out behaviour share only the pull-out load up to complete debonding P_1 48, then according to the tests carried out on DRAMIX hooked-end fibres P_1 = 30-55 N. P_1 could also be calculated using an analytical study by Naaman *et al.* 65 which is outside the scope of this work.

The pull-out load due to plastic hinges T_1 can be calculated for 3D fibres 47 as follows:

$$T_{1(3D)} = 2F_{PH}\left[1 + \frac{\mu \times \cos\beta}{1 - \mu \times \cos\beta}\right] / 1 - \mu \times \cos\beta \qquad (17)$$

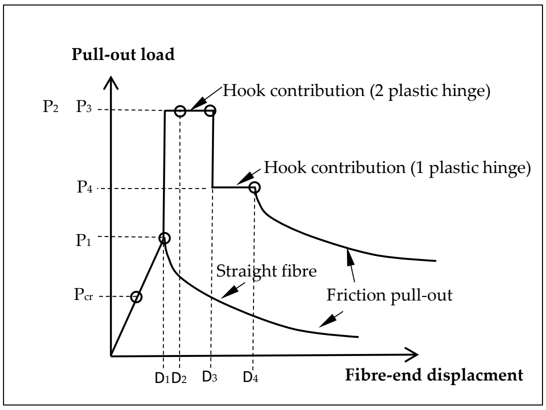

Figure 16. Sketch of the theoretical hooked-end 3D fibre pull-out adapted 47.

With μ as the coefficient of friction between concrete and steel taken as 0.5 and β was measured and shown in **Error! Reference source not found.**. Using Eq. (17), F_{PH} can be calculated and compared to that from Eq. (13). If the experimental F_{PH} from Eq. (17) is higher than the theoretical one calculated using Eq. (13), then the fibre was straightened following formation of 2 plastic hinges for 3D fibres.

Abdallah *et al.* 48 adapted this model to 4D and 5D fibres.

Eq. (16) remains valid for both 4D and 5D since P_1 load was similar. By applying the pulley model in a similar manner to Eq. (17), as depcited in Figs 17 and 18, the pull-out load due to plastic hinges T_1 can be calculated for 4D and 5D fibres as follows:

$$T_{1(4D)} = F_{PH}\left[3 + \left(\frac{2\mu \times \cos\beta}{1 - \mu \times \cos\beta}\right)\left[2\left(1 + \frac{\mu \times \cos\beta}{1 - \mu \times \cos\beta}\right) + 1\right]\right] / 1 - \mu \times \cos\beta \qquad (18)$$

$$T_{1(5D)} = F_{PH}\left[4 + \left(\frac{2\mu \times \cos\beta}{1 - \mu \times \cos\beta}\right)\left[3 + 2\mu\cos\beta\left[2\left(1 + \frac{\mu \times \cos\beta}{1 - \mu \times \cos\beta}\right) + 1\right] + 2\left(1 + \frac{\mu \times \cos\beta}{1 - \mu \times \cos\beta}\right) + 1\right]\right] / 1 - \mu \times \cos\beta \qquad (19)$$

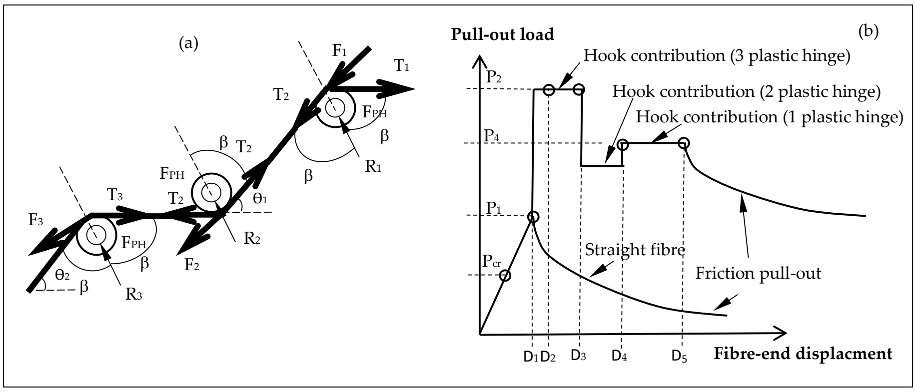

Figure 17. a- Pulley model for 4D fibres b- theoretical hooked-end 4D fibre pull-out load-slip adapted from 48.

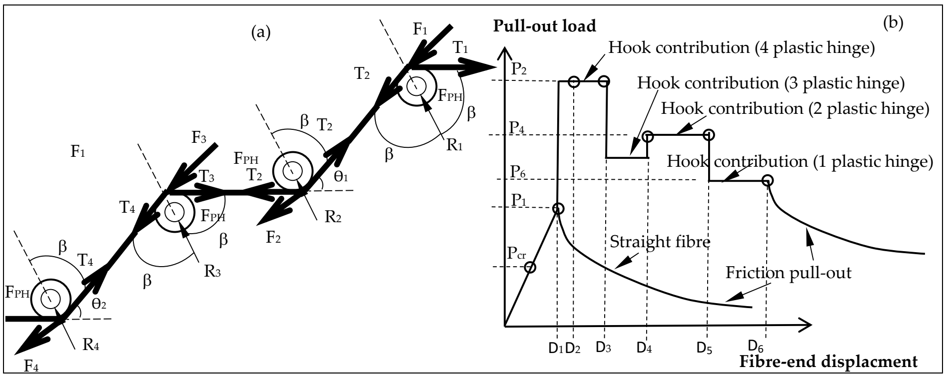

Figure 18. a- Pulley model for 5D fibres b- Theoretical hooked-end 5D fibre pull-out load-slip adapted from 48.

Error! Reference source not found. shows that the theoretical model to calculate M_P in Eq. (14) suggested by Alwan *et al.* 47 seems to overestimate the behaviour of pull-out since $F_{PH,theoretical} > F_{PH,test}$ for all fibres, which translates into fibres not becoming straightened at the end of the test. Given that all fibres with the exception of 5D were straightened by the end of the test, a new Equation (20) was proposed to calculate M_P which considers the comparatively weak lightweight concrete and its porous nature. This equation assumes that the effective distance between the centroids of tension and compression forces in a plastic stress distribution diagram for steel fibre circular section is $\frac{2r_f\pi}{15}$ ($\frac{2r_f}{3}$ for Alwan *et al.* 47 model and the true distance $\frac{8r_f}{3\pi}$ for Abdallah *et al.* 48 model). Thus, for the porous lightweight concrete, fibres were assumed to not undergo heavy straining after developing plastic hinges before becoming straightened and eventually pulling out.

$$M_P = f_y \cdot \pi r_f^2/2 \cdot d_f/3 \cdot \pi/5 \quad (20)$$

As seen in **Error! Reference source not found.**, the new model marginally underestimates the value of F_{PH} by a maximum of 3% for 3D, 3D** and 4D fibres while predicting that they become straightened ($F_{PH,theoretical} < F_{PH,test}$). On the other hand, the 5D fibre clearly does not become straightened according to this model. It should be noted that while the majority of 5D specimens appeared to be completely unstraightened, some 5D specimens looked partially straightened.

Table 6. Summary of experimental and theoretical F_{PH} values.

Type of fibre	$F_{PH,test}$ (N)	$F_{PH,theoretical}$ (N) Alwan *et al.* (1999)	$F_{PH,theoretical}$ (N) Proposed
3D	73.8	117.6	72.1
3D**	31.5	42.8	31.1
4D	131.2	214.2	129.7
5D	90.5	265.4	166.7

Considering the preceding discussion, it is safe to assume that unless the concrete is of high strength and therefore capable of providing strong fibre-matrix interfacial bond, such as the ultra-high strength concrete tested by Abdallah *et al.* 48, it is recommended that multiple-bend fibres with high tensile strength (such as 5D fibres) should not be employed as reinforcement for concrete with low concrete grade, since they might cause local fracturing during fibre straightening process. Given that there exists a possibility of matrix fracture due to 5D fibres not fully developing plastic hinges and becoming straightened, 4D and 3D* fibres appear to be the most efficient fibres for use in the LWAC sampled tested depending on their structural usage, with the aspect ratio a_f playing a significant role in bond strength efficiency while the number of hooks having more impact on energy dissipation efficiency. Finally, it could be argued that 4D fibres with higher a_f would further increase the efficiency indices and thus enhance the behaviour of SFRLC.

4.4. Proposed Constitutive Tensile σ-ω Model

Although it cannot be used directly for engineering calculations such as beam section analysis, the tensile stress-crack width (σ-ω) relationship is preferred to the stress-strain (σ-ε) relationship because it represents the actual behaviour of the fibrous material especially after cracking. It is derived from analysing the output results of the uniaxial tensile test, is member size-effect independent, and can be directly applied from the pull-out tests used to FEM 66. Also, the σ-ω relationship can provide the necessary information needed to design for the serviceability limit state, including fatigue and shrinkage. To be able to use the σ-ε relationship for section analysis based on the pull-out tests, the strain values are derived using the crack width and the structural characteristic length l_{cs} (using the relation $\varepsilon = \omega / l_{cs}$), which varies depending on specimen size, V_f, fibre type, reinforcement, loading level and matrix strength. No agreement has yet been achieved to determine l_{cs}, however for beams, l_{cs} can be chosen as the minimum of s_{rm} and h_{sp}, where s_{rm} is the mean distance between cracks, and h_{sp} is the unnotched depth 66,67. It should be noted that the proposed model ignores the slight drop in load following matrix cracking which lasted in the range of 0.05 to 0.1 mm slip before the load was increased. This was deemed of negligible practical impact on the accuracy of σ-ω relationship. **Error! Reference source not found.** depicts the idealised proposed multilinear stress-crack width relationship based on the uniaxial tensile pull-out tests for 3D fibres.

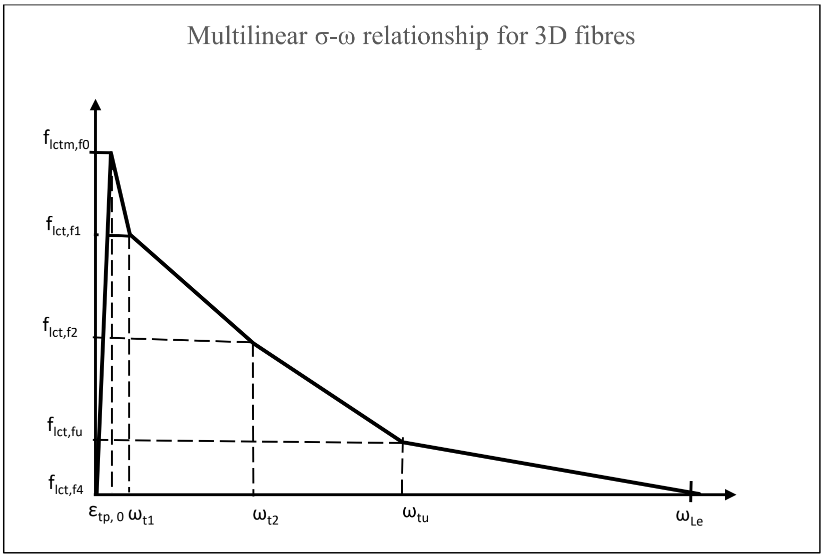

Figure 19. Multilinear σ-ω relationship for 3D fibres.

Due to the sensitivity of the pull-out machine, the accuracy of measuring the early slip pre-peak was somewhat limited. Hence, the rule of fibrous composites was adopted to determine the strain at peak before cracking for plain concrete ε_{tp}. The Young's modulus of Elasticity of the concrete in tension:

$$E_{ct} = E_{mt}V_m + \eta_l\eta_o E_f V_f \quad (21)$$

where E_{mt} and E_f are the plain concrete matrix and fibre's Young's moduli of Elasticity in tension, respectively; V_m and V_f are the volume fractions of the matrix and fibres, respectively; η_l is the fibre length efficiency and η_0 is the fibre orientation factor.

Similarly to Lok and Xiao 60, it is assumed that the initial modulus of elasticity in tension is equal to that in compression. Hence:

$$E_{mt} = E_c \quad (22)$$

Also, based on the pull-out tests, it was evident that σ_f was low since a relatively negligible increase or decrease in the uniaxial tensile strength of the concrete was recorded pre-crack for fibrous concrete specimens. Once cracking took place, the load abruptly degraded, followed by mobilisation of the fibre crack arresting effect. Therefore, before cracking takes place, Eq. (21) with $V_m \sim 1$, becomes:

$$E_{ct} \approx E_c \quad (23)$$

The strain at peak can now be calculated below with $f_{lctm,p}$ is the stress of the plain concrete.

$$\varepsilon_{tp} = f_{lctm,p}/E_{ct} \quad (24)$$

As previously shown in the pull-out tests, the uniaxial tensile stress at which the crack took place for SFRLC was similar to that of the plain lightweight concrete. The stress due to fibres immediately before cracking can be estimated using the following equation:

$$f_{lctm,f0} = f_{lctm,p} \quad (25)$$

Plain lightweight concrete uniaxial tensile stress can be written as:

$$f_{lctm,p} = 0.26 f_{lcm}^{2/3} \times (0.4 + 0.6\,\rho/2200) \quad (26)$$

Eq. (26) was adapted from Eurocode 2 68, where f_{lcm} (MPa) is the mean compressive strength of lightweight concrete based on the cylinder compression tests and ϱ is the oven density of concrete (kg/m^3). Using the above equation, R^2 was found to be 0.96.

From **Error! Reference source not found.**, the first residual uniaxial tensile stress $f_{lct,f1}$ of SFRLC which takes place after cracking as peak of either tension hardening or softening, can be derived using Eq. (4) from the pull-out test or regression Eq. (27) (R^2 = 0.95). The crack width ω_{t1} at $f_{lct,f1}$ varied for all the SFRLC specimens, with specimens having stronger fibres showing the highest ω_{t1}. For the majority of specimens, ω_{t1} ranged from 0.4 to 0.5 mm for 3D, 0.5 to 0.8 mm for 4D and 1.1 to 1.4 mm for 5D. This largely agrees with Abdallah *et al.* 58 pull-out tests on normal strength concrete of 33 MPa. The residual slip ω_{t1} can also be calculated based on the following regression Eq. (28) (R^2 = 0.89). The fibre reinforcing factor $\rho_f = V_f(L_f + L_e)/d_f\ (\delta \cdot \kappa)$ detailed elsewhere and $\varrho'_f = \varrho_f$ (for V_f = 1%).

$$f_{lct,f1} = \eta_0 V_f f_{lctm,p} \rho'_f \left(172.1 + 35.5 f_{lctm,p} \rho'_f\right) \quad (27)$$

$$\omega_{t1} = 0.2124 \rho_f'^2 + 0.3775 \rho'_f \quad (28)$$

Using the idealised stress-crack width relationship in **Error! Reference source not found.**, the load drops at a further slip of 2 mm to 3 mm. This was denoted as ω_{t2}. After thorough inspection of the pull-out tests, ω_{t2} was deemed to be approximately equal to the hook arm L_2 shown in **Error! Reference source not found.**. The observation that $\omega_{t2} = L_2$ is also supported by the work carried out on hooked end fibres by 47 and recent revisions from Abdallah *et al.* 58 pulley model on DRAMIX hooked-end 3D, 4D and 5D fibres. In the latter paper, after fibre debonding 2 plastic hinges were developed for 3D fibres (3 plastic hinges for 4D and 4 plastic hinges for 5D fibres). At this stage, the second residual pull-out stress due to fibre contribution was recorded. Once the slip reaches L_2, the mechanical anchorage mechanism becomes supported by only 1 plastic hinge for 3D fibres, 2 for 4D fibres and 3 for 5D fibres, which therefore results in a significant drop in the pull-out load. From the pull-out tests, the second residual pull-out stress $f_{lct,f2}$ recorded at $\omega_{t2} = L_2$ was in the range of 30 to 40% lower than $f_{lct,f1}$ for all the 3D, 4D and 5D specimens. Thus, for design purposes:

$$f_{lct,f2} = 0.60 \times f_{lct,f1} \quad (29)$$

When the crack width $\omega_{tu} = L_h$ (the full length of the hook), the load drops significantly and only frictional pull-out becomes thereafter responsible for the SFRLC behaviour, while 1 plastic hinge and 2 plastic hinges remain responsible for 4D and 5D behaviours, respectively. Hence, at $\omega_{tu} = L_h$, the load drops to about 10 to 25% for all the specimens tested and frictional pull-out starts to take place. Thus, the stress $f_{lct,fu}$ can be written as:

$$f_{lct,fu} = 0.10 \times f_{lct,f1} \quad (30)$$

It is vital that the hook of the fibre is fully embedded in concrete for the fibrous mix to develop the maximum residual stress $f_{lct,f1}$, hence the final crack width can be written as:

$$\omega_{Le} = L_e = L_h + 5d_f \quad (31)$$

where ω_{Le} is the effective length crack width in (mm). For Design purposes the ultimate tensile strength $f_{lct,f4}$ can be assumed to be 0.

A similar semi-empirical approach can be adopted to derive the tensile behaviour of 4D and 5D fibres. The proposed multilinear uniaxial tensile σ-ω relationships suggested are specific to the type of fibre used and depend on experimental strength reduction factors fully based on the pull-out tests. Hence, these reasons render the models laborious and reliant on uniaxial tensile tests. In order to make the model more generic (covering hooked-end, crimped or straight fibres embedded in concrete matrices with different strengths), easy to use and to avoid any reliability on the pull-out or uniaxial tensile tests, the generic model in **Error! Reference source not found.** is suggested.

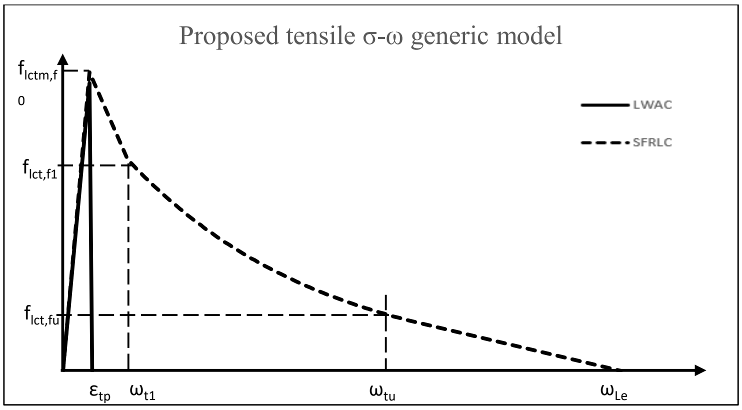

Figure 20. Proposed generic constitutive σ-ω model for plain and fibrous lightweight concrete.

The tensile stress in **Error! Reference source not found.** is explained in the equations below.

$$f_{lct} = \begin{cases} E_{ct} \cdot \varepsilon_t & \text{if } \varepsilon_t \leq \varepsilon_{tp} \\ f_{lctm,f0} + (f_{lct,f1} - f_{lctm,f0})\omega_t/\omega_{t1} & \text{if } 0 < \omega_t \leq \omega_{t1} \\ f_{lct,f1} e^{-\zeta} & \text{if } \omega_{t1} < \omega_t \leq \omega_{tu} \end{cases} \quad (32)$$

$$\zeta = (\omega_t - \omega_{t1})/\omega_{tu} \cdot n_b/\rho_f \quad (33)$$

The tensile stress should be 0 at ω_{Le}. ω_{tu} is L_h for hooked end fibre, length of one wave or turn of the crimped fibres and length of straight fibre/10. n_b is the number of bends in one hook (1 for 3D, 2 for 4D and 3 for 5D). n_b is taken as half the total number of waves for crimped fibres (usually 4 or 3), and 5 for straight fibres.

4.5. Validation of the Tensile σ-ω Model

In order to validate the proposed model above, the average experimental uniaxial tensile behaviours of 3D, 4D and 5D fibrous specimens are shown against the predictions of the proposed model in **Error! Reference source not found.**.

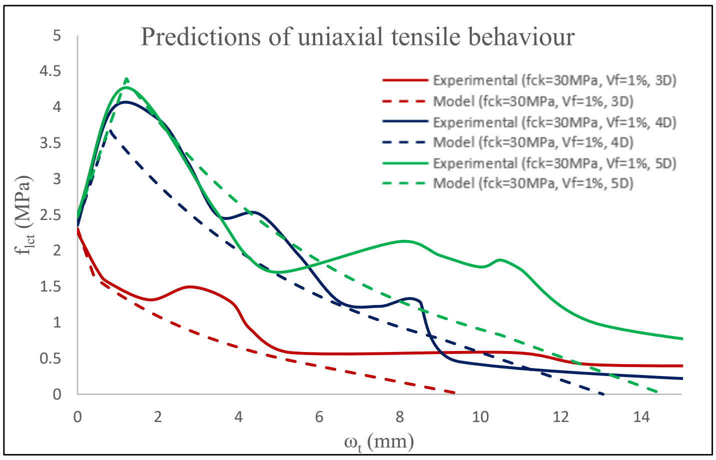

Figure 21. Predicted behaviour of uniaxial tension for 3 different specimens.

It can be seen that the proposed tensile σ-ω model predicted the uniaxial tensile behaviour of different fibrous specimens with good accuracy. For 3D and 4D specimens, the first residual tensile stress $f_{lct,f1}$ was underestimated by 4% and 6%, respectively, while for 5D specimen an overestimation of 2% was noted. The predicted slip ω_{t1} was within 20% of the actual one. However, this inaccuracy in slip predictions was on the conservative side and can be blamed for by the high variability in slip results stemmed from the nature of the pull-out test. This observation was also reported by Barragán *et al.* 57, who conducted uniaxial tensile tests on SFRC (3D fibres) cylinders with comparable strengths of 30 MPa to the notched prisms tested. The proposed constitutive model assumes that the ultimate crack width is the minimum required for adequate embedment of hooks (equivalent to the effective embedment length $\omega_{Le} = L_e = L_h + 5d_f$), which enables the development of the bond required to fully straighten the fibres. For this reason, the final slip predictions were conservative as the experimental uniaxial tensile behaviour was based on pull-out specimens with an embedment length L_E of around 25 mm which is larger than L_e. Hence, although conservative during the post-peak, the suggested model is seen to be successful at predicting the tensile σ-ω behaviour of the tested specimens.

As previously discussed in Section **Error! Reference source not found.**, only a handful of research work on the uniaxial tensile stress-strain or stress-crack width behaviour of SFRLC exists. De Montaignac *et al.* 66 work on the tensile behaviour of SFRC notched cylinders was investigated. De Montaignac *et al.* 66 carried out uniaxial tensile notched cylinders tests according to RILEM TC 162-TDF 42 on normal weight concrete of strength ranging from 45 to 63 MPa reinforced with 3D** and 3D* fibres, and generated uniaxial tensile σ-ω curves. Although, the concrete was not lightweight, it is interesting to check the reliability of the proposed uniaxial tensile σ-ω law since it mainly depends on the type of fibre and the plain concrete strength, which were provided by De Montaignac *et al.* 66.

Error! Reference source not found. shows the proposed constitutive model prediction of the experimental notched cylinders uniaxial tensile σ-ω behaviour for concrete reinforced with 3D* fibres of V_f = 1% from De Montaignac *et al*. (2011). It is evident that the proposed model was successful at predicting the uniaxial tensile behaviour of SFRC. The model underestimated the peak post-cracking tensile stress by only 3% and overestimated the residual stresses by an average of 5-10% after a crack width of 1.9 mm.

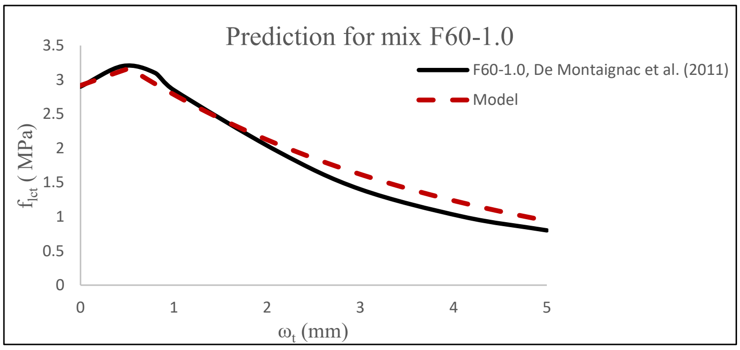

Figure 22. Prediction of 66 uniaxial stress-crack width behaviour of SFRC notched cylinders reinforced with 3D* fibres of V_f = 1%.

Error! Reference source not found. shows the proposed constitutive model prediction of the experimental notched cylinders uniaxial tensile σ-ω behaviour for concrete reinforced with 3D** fibres of V_f = 1% from De 66. As previously noted, the proposed model ignored the dip in stress which takes place at 0.1 mm slip after cracking, commonly observed in uniaxial tests such as this one and 57. This should have little to no effect on the prediction of the behaviour of load-deflection of structural elements using the structural characteristic length l_{cs} to derive strain (such as in 67). The proposed constitutive σ-ω model predicted the uniaxial tensile behaviour of SFRC with good accuracy and was conservative by an average of 8-12% at all levels.

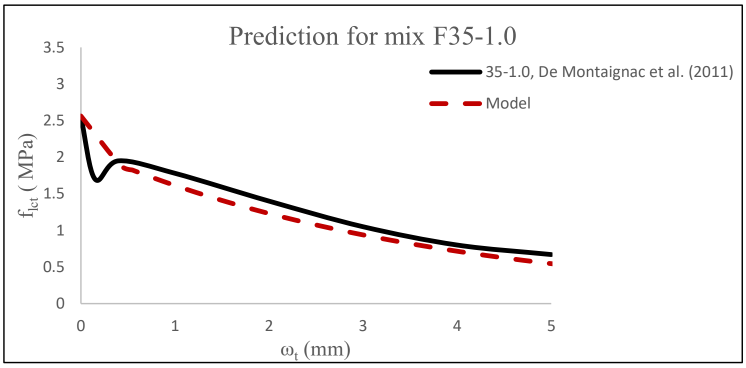

Figure 23. Prediction of 66 uniaxial stress-crack width behaviour of SFRC notched cylinders reinforced with 3D** fibres of V_f = 1%.

4.6. Fracture Energy G_f

Using the proposed tensile constitutive σ-ω relationship based on the pull-out experiments, the fracture energy of the fibrous mixes can be calculated using:

$$G_F = \int_{\omega_c=0}^{\omega_{L_E}} f_{lct}\,(\omega)dw \qquad (34)$$

G_F for each of the mixes is summarised **Error! Reference source not found.** for concrete of f_{lck} = 30 MPa. It could be observed that the main reasons behind the differences in G_F values are the number of bends n_b, fibre hook length and fibre volume fraction. The larger n_b, hook length and V_f, the more the energy absorbed to deform and straighten the fibre and hence the higher the fracture energy G_F produced per unit width of crack. From **Error! Reference source not found.**, it can be seen that the highest G_F is generated by samples with 4D and 5D fibres, while those with 3D** fibres generated the lowest G_F. It was not possible to calculate the fracture energy for plain lightweight concrete as the machine was not stiff enough to record the insignificant crack width recorded following concrete cracking using the uniaxial tensile pull-out test.

Table 7. Fracture energy based on the proposed constitutive uniaxial tensile model.

Fibre type	V_f	G_F (N/mm)
3D	1%	5393
	2%	13253
4D	1%	17433
	2%	44892
5D	1%	23563
	2%	60589
3D*	1%	9389
	2%	22045

3D**	1%	4872
	2%	11654

4.7. Conclusions

In the present experimental investigation, a direct tensile test was designed to examine the pull-out load-slip and uniaxial tensile behaviour of recycled lightweight aggregate concrete. Severasl parameters were included in the study, such as fibre geometry (n_b, a_f, L_f), volume fraction V_f and compressive strengths f_{lck}. It can be concluded that:

- The designed pull-out test showed a truer representation of a tensile crack being bridged by fibres on the macro level in a structural member. Also, using the area of the notch in which the fibre(s) was embedded, it was possible to regard the pull-out test as a uniaxial tensile test of plain and fibrous lightweight concrete.
- Due to the absence of a natural tension-stiffening mechanism, plain lightweight concrete was found to fail in a sudden brittle manner once it reached its peak tensile strength. The addition of fibres to lightweight concrete was seen to drastically enhance both tensile strength and ductility including work and fracture energy, once the main tensile crack was initiated. Before the latter took place, a negligible increase in strength was seen. The higher the number of fibre bends n_b, fibre aspect ratio a_f, fibre length L_f, fibre dosage V_f and plain concrete compressive strength f_{lck}, the higher the post-cracking tensile strength and ductility of the fibrous composite. The embedded length L_E was found to only enhance ductility of SFRLC. It was found that a minimum value of $L_E = L_h + 5d_f$ is required for the hooked-end fibres to bond adequately and develop maximum pull-out load P_{max}. Also, although the increase in fibre inclination angle Θ_f was found to increase post-cracking tensile strength as compared to $\Theta_f = 0°$, in some instances where $\Theta_f = 45°$, the concrete fractured. An inclination angle of about 20° was found to add tensile strength without compromising ductility. It was found that smooth fibres were ineffective at increasing strength of SFRLC and merely enhanced ductility via frictional pull-out.
- A new ultimate bond strength equation to quantify the behaviour of hooked-end steel fibres in lightweight concrete was suggested based on the pull-out tests. It was found that 4D fibres showed the highest bond strength while 3D** showed the lowest bond strength. Also, the maximum uniaxial tensile stress for SFRLC specimens was determined while taking into consideration the random distribution of fibres in a practical situation.
- A fibre optimisation study was carried out and concluded that incorporating multiple-bend fibres such as 5D which also had a high tensile strength of 2300 MPa, with concrete of strength of 30 MPa can cause local fracturing of lightweight concrete matrix. This is attributed to the difficulty of concrete to allow plastic hinge formation then straightening of the fibre during the pull-out process. Hence, it is advised that 5D fibres should not be employed as reinforcement for concrete of low grade. Also, 3D* and 4D fibres appeared to be the most efficient and optimum for reinforcing the lightweight concrete tested of strengths of 30-45 MPa, with the aspect ratio a_f playing a significant role in bond strength efficiency while the number of bends n_b having more impact on energy dissipation efficiency.
- A semi-empirical constitutive tensile stress-crack width (σ-ω) model for fibrous lightweight concrete based on the experimental testing was derived. The equations defining the residual tensile strengths $f_{lct,f1}$ and crack widths ω_{t1} were based on regression analysis. The model showed its success at predicting the uniaxial tensile behaviour of SFRLC specimens. Since the model relies on fibre reinforcing factor ϱ_f (which is based on fibre geometry and fibre volume fraction), and plain compressive or tensile

strength, the model was also capable of validating the uniaxial tensile behaviour of steel-fibre-reinforced normal weight concrete from previous literature.

- The benefits of steel fibres in addressing the brittlness of lightweight concrete is of particular interest to designers and practitioners. This is in addition to the construction time savings from using fibres (which are simply added to the mix, as opposed to steel laying). Using recycled-waste-based aggregates alongside fibres also adds to these practical benefits. The proposed constitutive model will allow designers to carry out more detailed analysis and design simulations in order to better understand the structural responses.
- In terms of future work, more research on SFRLC needs to be carried out at the structural level to include a comprehensive experimental testing programme of structural beams of different boundary and loading conditions, cross sections, spans, and shear configurations. Numerical modelling can also be performed using the proposed material model. Some structural testing and finite-element analyses have been already undertaken, which will be reported in follow-up articles. The long-term behaviour of fibrous concrete remains largely unquantified by current standards, so this will benefit from further examination.

Notation

flck,cube	characteristic cube compressive stress
flck	characteristic cylinder compressive stress
flc	cylinder compressive stress
flcm	mean compressive cylinder stress
flcm,p	mean compressive cylinder stress of plain concrete
flcm,cube	mean cube compressive stress
$f_{lctm,m}$	maximum uniaxial tensile stress
A_f	area of a single fibre
d_f	fibre diamter
Elcm	mean value of Young's modulus of elasticity
Elcm,f	peak elastic modulus of SFRLC
nb	number of bends
df	diameter of fibre
Le	effective fibre anchorage length
LE	embedded length of fibre
Lf	length of fibre
κ	fibre material factor
ϱf	fibre reinforcing factor
δ	fibre shape factor
P_{max}	maximum pull-out strength for a single fibre
V_f	fibre volume fraction
W_p	total work done by fibre
μlc	Poisson's ratio
ε	strain
εlc1	strain at peak compressive stress of LWAC
εlcf	strain at peak compressive stress of SFRLC
εt1	strain at post-cracking first residual tensile stress
εlcu	strain at ultimate compressive stress of LWAC
εlcf,ult	strain at ultimate compressive stress of SFRLC
η_0	fibre orientation factor
σ_f	fibre stress
τ_{av}	fibre-matrix interfacial bond shear stress
τ_{ult}	ultimate bond strenght of SFRLC matrix
σ	stress
$\sigma_{av,f}$	average stress of fibre

σ_c	average stress of concrete
σ_y	fibre yield stress
σ_u	fibre ultimate stress
Ef	Young's modulus of elasticity fibre
SFRLC	Steel Fibre Reinforced Lightweight Concrete
LWAC	Lightweight Aggregate Concrete

References

1. Al-Khaiat, H., and Haque, M.N. (1998). Effect of initial curing on early strength and physical properties of lightweight concrete. Cement and Concrete Research 28, 859–866.
2. Gerritse, A. (1981). Design considerations for reinforced lightweight concrete. International Journal of Cement Composites and Lightweight Concrete, 3(1), pp.57-69.
3. Lyag (2011). Technical manual. London: Lytag ltd.
4. Lytag. (2014). Ramboll Frame Comparison Study. Available: https://www.aggregate.com/our-businesses/lytag. Last accessed 31st Dec 2019.
5. Chandra, S., and Berntsson, L. 2003. Lightweight Aggregate Concrete Science. Technology and Applications. Standard Publishers Distributors, Delhi, India, ISBN 81-8014-052-0.
6. Ahn, Y.B., Jang, J.G., and Lee, H.K. (2016). Mechanical properties of lightweight concrete made with coal ashes after exposure to elevated temperatures. Cement & Concrete Composites 72: 27–38.
7. Libre, N.A., Shekarchi, M., Mahoutian, M., and Soroushian, P. (2011). Mechanical properties of hybrid fiber reinforced lightweight aggregate concrete made with natural pumice. Construction and Building Materials, 25(5), pp.2458-2464.
8. Campione, G. (2014). Flexural and Shear Resistance of Steel Fiber–Reinforced Lightweight Concrete Beams. Journal of Structural Engineering, 140 (4), 1-8.
9. Dias-da-Costa, D., Carmo, R.N.F., Graça-e-Costa, R., Valença, J., and Alfaiate, J. (2014). Longitudinal reinforcement ratio in lightweight aggregate concrete beams. Engineering Structures. 81, 219–229.
10. Mo, K.M., Goh, S., Alengaram, U., Visintin, P. and Jumaat, M. (2017). Mechanical, toughness, bond and durability-related properties of lightweight concrete reinforced with steel fibres. Materials and Structures, 50(1).
11. Lim, Wee, Mansur and Kong. (2006). Flexural behavior of reinforced lightweight aggregate concrete beams. In: Asia-Pacific Structural Engineering and Construction Conference. Kuala Lumpur: APSEC, pp.68-82.
12. Chen, H., Huang, C. and Tang, C. (2010). Dynamic Properties of Lightweight Concrete Beams Made by Sedimentary Lightweight Aggregate. Journal of Materials in Civil Engineering, 22 (6), 599-606.
13. Wu, C., Kan, Y., Huang, C., Yen, T. and Chen, L. (2011). Flexural behavior and size effect of full scale reinforced lightweight concrete beam. Journal of Marine Science and Technology, 19(2), 132-140.
14. Badogiannis, E., and Kotsovos, M. (2014). Monotonic and cyclic flexural tests on lightweight aggregate concrete beams. Earthquakes and Structures, 6(3), pp.317-334.
15. Lambert, G., "Properties and Behaviour of Structural Lightweight (Lytag - Sand) Concrete", Ph.D, University of Sheffield (1982).
16. Lo, T.Y, Cui, H., Memon, S.A., and Noguchi, T. (2016). Manufacturing of sintered lightweight aggregate using high-carbon fly ash and its effect on the mechanical properties and microstructure of concrete. Journal of Cleaner Production 112: 753–762.
17. Bilodeau, A., Kodur, V. and Hoff, G. (2004). Optimization of the type and amount of polypropylene fibres for preventing the spalling of lightweight concrete subjected to hydrocarbon fire. Cement and Concrete Composites, 26(2), pp.163-174.
18. Collins, R. and Sherwood, P. (1995). Use of waste and recycled materials as aggregates. London: H.M.S.O.
19. Gao, J., Sun, W. and Morino, K. (1997). Mechanical properties of steel fiber-reinforced, high-strength, lightweight concrete. Cement and Concrete Composites, 19(4), pp.307-313.
20. Campione, G. and La Mendola, L. (2004). Behavior in compression of lightweight fiber reinforced concrete confined with transverse steel reinforcement. Cement and Concrete Composites, 26 (6), 645-656.
21. Abbas, A.A, Syed Mohsin, S.M., Cotsovos, D.M. (2014). Seismic response of steel fibre reinforced concrete beam–column joints. Engineering Structures, 59, pp.261-283.
22. Di Prisco, M., Colombo, M. and Dozio, D. (2013). Fibre-reinforced concrete in fib Model Code 2010: principles, models and test validation. Structural Concrete, 14(4), pp.342-361.

23. Grabois, T.M., Cordeiro, G.C., and Filho, R.D.T. (2016). Fresh and hardened-state properties of self-compacting lightweight concrete reinforced with steel fibers. Construction and Building Materials, 104, pp.284-292.
24. Abbas, A.A., Syed Mohsin, S.M., Cotsovos, D.M., Ruiz-Teran, A.M. (2014). Shear behaviour of SFRC simply-supported beams, ICE Proc. Structures and Buildings, 167(SB9), pp. 544-558, DOI: https://doi.org/10.1680/stbu.12.00068.
25. Abbas, A.A., Syed Mohsin, S.M., Cotsovos, D.M. (2014). Seismic response of steel fibre reinforced concrete beam-column joints, Engineering Structures, 59, pp. 261-283, DOI: https://doi.org/10.1016/j.engstruct.2013.10.046.
26. Ritchie A., Kayali O. (1975). The effects of fiber reinforcement on lightweight aggregate concrete. In: Neville A (ed.), Proceedings of RILEM Symposium on Fiber Reinforced Cement and Concrete, The Construction Press Ltd, 247–256.
27. Swamy, N., Jones, R. and Chiam, A. (1993). Influence of Steel fibers on the Shear Resistance of Lightweight Concrete I-Beams. ACI Structural Journal, 90(1).103-114.
28. Kang, T. and Kim, W. (2010). Shear strength of steel fiber-reinforced lightweight concrete beams. Oklahoma: Korea Concrete Institute, pp.1386-1392.
29. Iqbal, S., Ali, A., Holschemacher, K. and Bier, T. (2015). Mechanical properties of steel fiber reinforced high strength lightweight self-compacting concrete (SHLSCC). Construction and Building Materials, 98, pp.325-333.
30. Al-Naimi, H. (2020). Structural behaviour of steel fibre reinforced lightweight concrete, PhD, London.
31. Al-Naimi, H.K., Abbas, A.A. (2023). Constitutive model for plain and steel-fibre-reinforced lightweight concrete under compression. Structural Concrete, 24(6), pp. 7625–7647. DOI: https://doi.org/10.1002/suco.202200646.
32. IEA. (2019). *World energy outlook 2019*. Available: https://www.iea.org/reports/world-energy-outlook-2019/coal#abstract. Last accessed 1st Oct 2020.
33. Kotsovos, M.D. and Pavlović, M.N., 1995. Structural concrete, Finite-element analysis for limit-state design. London. Thomas Telford.
34. Löfgren, I. (2005). Fibre-reinforced Concrete for Industrial Construction: a fracture mechanics approach to material testing and structural analysis. Ph.D. CHALMERS UNIVERSITY OF TECHNOLOGY, Göteborg, Sweden.
35. Lee, S.-C., Cho, J.-Y., and Vecchio, F. J. (2011). Diverse Embedment Model for Steel Fiber-Reinforced Concrete in Tension: Model Development. ACI materials journal. 108 (5), 516-525.
36. Kayali, O., Haque, M. and Zhu, B. (2003). Some characteristics of high strength fiber reinforced lightweight aggregate concrete. Cement and Concrete Composites, 25(2), pp.207-213.
37. Zhao, M., Zhao, M., Chen, M., Li, J., Law, D. (2018). An experimental study on strength and toughness of steel fiber reinforced expanded-shale lightweight concrete. Construction and Building Materials. 183, 493–501.
38. Badogiannis, E.G., Christidis, K.I., Tzanetatos, G.E. (2019). Evaluation of the mechanical behavior of pumice lightweight concrete reinforced with steel and polypropylene fibers. Construction and Building Materials. 196, 443–456.
39. Liu, Xi., Wu, Tao., and Liu, Y . (2019). Stress-strain relationship for plain and fibre-reinforced lightweight aggregate concrete. Construction and Building Materials. 225, 256-272.
40. Mo, K.M, Yap, K.K.Q, Alengaram, U.J, Jumaat, M.Z. (2014). The effect of steel fibres on the enhancement of flexural and compressive toughness and fracture characteristics of oil palm shell concrete. Construction and Building Materials. 55, 20-28.
41. ASTM D638-10 (2014) Standard Test Method for Tensile Properties of Plastics. ASTM International, West Conshohocken.
42. RILEM TC 162-TDF (2001): Test and design methods for steel fibre reinforced concrete. Recommendations for uni-axial tension test. Materials and Structures 34, Jan-Feb 2001, pp. 3-6.
43. Abdallah, S., Rees, D.W.A, Hamidreza, S., and Fan, M. (2018). Understanding the effects of hooked-end steel fibre geometry on the uniaxial tensile behaviour of self-compacting concrete. Construction and Building Materials. 178, 484-494.
44. Abdallah, S., Fan, M., and Zhou, X. (2016a). Effect of Hooked-End Steel Fibres Geometry on Pull-Out Behaviour of Ultra-High Performance Concrete. International Journal of Civil, Environmental, Structural, Construction and Architectural Engineering. 10 (12), 1594-1599.
45. Bekaert, 2020, <https://www.bekaert.com/en/> (20 June 2020).
46. Robins, P., Austin, S., and Jones, P. (2002). Pull-out Behaviour of Hooked Steel Fibres. Materials and Structures, RILEM, 35, 434-442.
47. Alwan, J., Naaman, A. and Guerrero, P. (1999). Effect of mechanical clamping on the pull-out response of hooked steel fibers embedded in cementitious matrices. Concrete Science and Engineering, 1, pp.15-25.
48. Abdallah, S., Fan, M., and Rees, D.W.A. (2016b). Analysis and modelling of mechanical anchorage of 4D/5D hooked end steel fibres. Materials and Design. 112, 539–552.

49. Abdallah, S., Fan, M., and Zhou, X. (2017). Pull-Out Behaviour of Hooked End Steel Fibres Embedded in Ultra-high Performance Mortar with Various W/B Ratios. International Journal of Concrete Structures and Materials. 11 (2), 301–313.
50. Romualdi, J.P., and Mandel, J.A. (1964). Tensile Strength of Concrete Affected by Uniformly Distributed and Closely Spaced Short Length of Wire Reinforcement. AC1 JOURNAL, Proceedings 61 (6), 657-671.
51. Krenchel, H., 'Fibre spacing and specific fibre surface' in 'Testing and Test Methods of Fibre Cement Composites', Proceedings of the RILEM Symposium, 1978 (Construction Press Ltd., Lancaster 1978) 69-79.
52. Soroushian, P., and Lee, C.-D. (1990b). Tensile Strength of Steel Fiber Reinforced Concrete: Correlation with Some Measures of Fiber Spacing. ACI materials journal. 87 (6), 541-546.
53. Wille, K., & Naaman, A. E. (2012). Pullout behavior of highstrength steel fibers embedded in ultra-high-performance concrete. ACI Materials Journal, 109(4), 479–588.
54. Wille, K., & Naaman, A. E. (2013). Effect of ultra-high-performance concrete on pullout behavior of high-strength brass-coated straight steel fibers. ACI Materials Journal, 110(4), 451–462.
55. Cao, Y.Y.Y., Yu, Q.L. (2018). Effect on inclination angle on hooked end steel fiber pull out behavior in ultra-high performance concrete. *Composite Structures*. 201, 151-160.
56. Qi, J., Wu, Z., Ma, Z.J., Wang, J. (2018). Pullout behaviour of straight and hooked-end steel fibers in UHPC matrix with various embedded angles. Construction and Building Materials. 191, 764-774.
57. Barragán, B.E., Gettu, R., Martín, M.A., Zerbino, R.L (2003). Uniaxial tension test for steel fibre reinforced concrete—A parametric study. Cem. Concr. Compos, 25: 767–777.
58. Abdallah, S., and Rees, D.W.A. (2019). Comparisons Between Pull-Out Behaviour of Various Hooked-End Fibres in Normal–High Strength Concretes. International Journal of Concrete Structures and Materials. 13, 1-15.
59. Lim, T.Y., Paramasivam, P., and Lee, S.L. (1987). Analytical Model for Tensile Behaviour of Steel-Fibre Concrete, ACI Materials Journal, Technical Paper, No 84- M30; p. 286 – 298.
60. Lok, T. and Xiao, J. (1998). Tensile behaviour and moment–curvature relationship of steel fibre reinforced concrete. Magazine of Concrete Research, 50(4), pp.359-368
61. Lok, T.-S. and Xiao, J.R. (1999): Flexural Strength Assessment of Steel Fiber Reinforced Concrete, Journal of Materials in Civil Engineering, Vol. 11 No. 3, August 1999, pp. 188-196.
62. Hannant, D.J. (1978). Fibre Cements and Fibre Concretes. John Wiley & Sons, Ltd.
63. Lee, S.-C., Cho, J.-Y., and Vecchio, F. J. (2011). Diverse Embedment Model for Steel Fiber-Reinforced Concrete in Tension: Model Development. ACI materials journal. 108 (5), 516-525.
64. Joo Kim, D. (2009). Strain rate effect on high performance fiber reinforced cementitious composites using slip hardening high strength deformed steel fibers.
65. Naaman, A. E., Namur, G. G., Alwan, J. M. and Najm, H. (1991). Fiber pull-out and bond slip, Part I: Analytical study. ASCE Journal of Structural Engineering. 117 (9), 2769-2790.
66. De Montaignac, R., Massicotte, B., Charron, J.-P. and Nour, A. (2011). Design of SFRC structural elements: post-cracking tensile strength measurement. Materials and Structures, 45(4), 609-622.
67. Fédération Internationale du béton (2013). fib model code for concrete structures 2010. Berlin: Ernst and Sohn. 147-150.
68. Comité Européen De Normalisation, 2004. Eurocode 2: Design of Concrete Structures - Part 1: General Rules and Rules for Buildings. British Standard, BS EN 1992:1:1.